Title
Simulating aerosols using a chemical transport model with assimilation of satellite aerosol retrievals: Methodology for INDOEX

Journal
Journal of Geophysical Research, 106(D7)

ISSN
0148-0227

Authors
Collins, William D
Rasch, Phillip J
Eaton, Brian E
et al.

Publication Date
2001-04-16

DOI
10.1029/2000jd900507

JOURNAL OF GEOPHYSICAL RESEARCH, VOL. 106, NO. D7, PAGES 7313–7336, APRIL 16, 2001

Simulating aerosols using a chemical transport model with assimilation of satellite aerosol retrievals: Methodology for INDOEX

William D. Collins, Phillip J. Rasch, Brian E. Eaton, Boris V. Khattatov, and Jean-Francois Lamarque
National Center for Atmospheric Research, Boulder, Colorado

Charles S. Zender
Earth System Science, University of California at Irvine, Irvine, California

Abstract. A system for simulating aerosols has been developed using a chemical transport model together with an assimilation of satellite aerosol retrievals. The methodology and model components are described in this paper, and the modeled distribution of aerosols for the Indian Ocean Experiment (INDOEX) is presented by *Rasch et al.* [this issue]. The system generated aerosol forecasts to guide deployment of ships and aircraft during INDOEX. The system consists of the Model of Atmospheric Transport and Chemistry (MATCH) combined with an assimilation package developed for applications in atmospheric chemistry. MATCH predicts the evolution of sulfate, carbonaceous, and mineral dust aerosols, and it diagnoses the distribution of sea salt aerosols. The model includes a detailed treatment of the sources, chemical transformation, transport, and deposition of the aerosol species. The aerosol forecasts involve a two-stage process. During the assimilation phase the total column aerosol optical depth (AOD) is estimated from the model aerosol fields. The model state is then adjusted to improve the agreement between the simulated AOD and satellite retrievals of AOD. During the subsequent integration phase the aerosol fields are evolved using meteorological fields from an external model. Comparison of the modeled AOD against estimates of the AOD from INDOEX Sun photometer data show that the differences in daily means are -0.03 ± 0.06. Although the initial application is limited to the Indian Ocean, the methodology could be extended to derive global aerosol analyses combining in situ and remotely sensed aerosol observations.

1. Introduction

Aerosols influence the present climate and affect future climate change by changing the planetary energy budget. The reflection and absorption of sunlight and terrestrial radiation by aerosols is termed direct radiative forcing, and the modification of cloud optical and microphysical properties by aerosols is termed indirect radiative forcing. Recent estimates of the direct radiative forcing by sulfate aerosols following the pioneering work of *Charlson et al.* [1992] have a central value of -0.4 W/m^2 with a factor of 2 uncertainty [*Intergovernmental Panel of Climate Change (IPCC)*, 1996]. The current consensus value for the direct radiative forcing by soot is $+0.1$ W/m^2 with a factor of 3 uncertainty. The indirect effect of aerosols [*Twomey et al.*, 1984] is the least well quantified, with estimates ranging from 0 to at least -1.5 W/m^2. The largest estimates of the radiative effects of aerosols are comparable to the climate forcing of 2.5 W/m^2 from greenhouse gases [*IPCC*, 1996]. The present uncertainties in the climate forcing by aerosols have hindered efforts to quantify climate change. The analysis is complicated by several factors, including the chemical and physical heterogeneity of aerosols, complex temporal, and geographic variation in the sources of aerosols and aerosol precursors, interaction of aerosols with the hydrologic cycle, and chemical transformation of aerosols. The reduction of these uncertainties is one of the primary focal points of current climate research [*Penner*, 1993].

Studies modeling the present-day climate forcing by aerosols have been based primarily upon chemical transport models (CTMs) and general circulation models (GCMs). CTMs are generally driven using meteorological fields obtained from an external source, for example, an operational meteorological analysis or GCM. CTMs have been used to study sulfate aerosols [*Kasibhatla et al.*, 1997], carbonaceous aerosols [*Liousse et al.*, 1996; *Cooke and Wilson*, 1996], mineral dust aerosols [*Tegen and Fung*, 1994; *Tegen and Lacis*, 1996], and combinations of sulfate, sea salt, and carbonaceous aerosols [*Tegen et al.*, 1997]. GCMs have been used to study direct forcing by sulfate and soot aerosols [*Haywood et al.*, 1997; *Kiehl et al.*, 2000], sea salt aerosols [*Gong et al.*, 1997a, 1997b], and more complex combinations of aerosol species.

Evaluation of the fidelity of these simulations has been hampered by sparse surface networks and the limitation of current satellite retrievals to oceanic regions. Large differences between various models and between models and observations suggest that an optimal aerosol model has not been developed to date. Global annual mean burdens of sulfate simulated by a

Paper number 2000JD900507.
0148-0227/01/2000JD900507$09.00

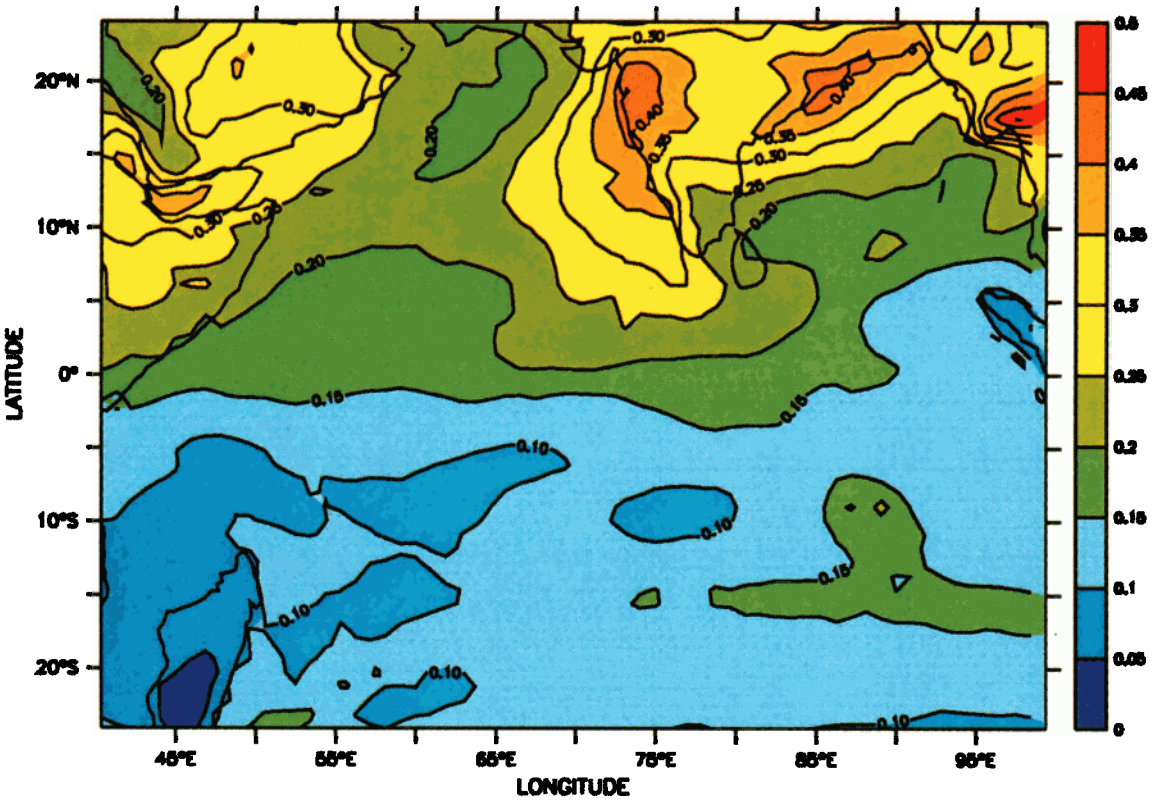

Plate 1. Average aerosol optical depth at $\lambda = 630$ nm for March 1–14, 1999, from the standard integration.

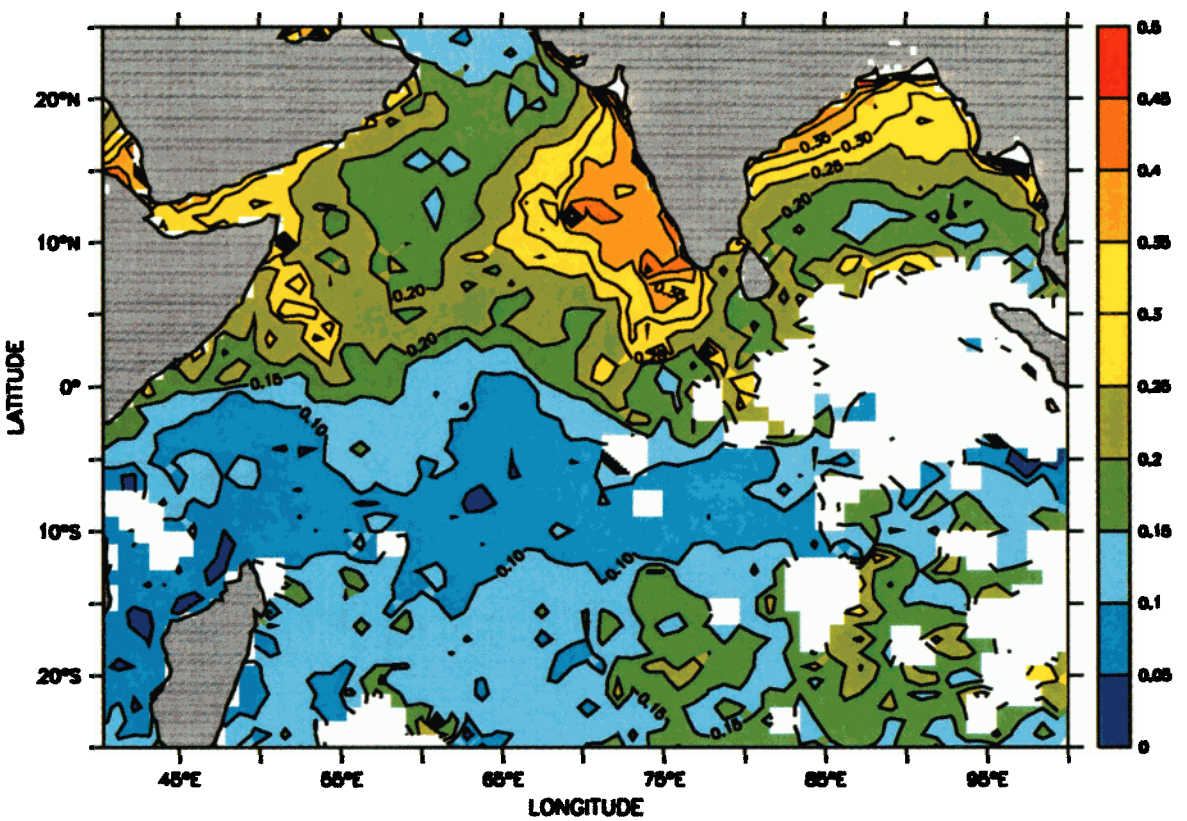

Plate 2. Average aerosol optical depth at $\lambda = 630$ nm for March 1–14, 1999, from the NOAA Pathfinder 2 algorithm applied to AVHRR data from NOAA-14.

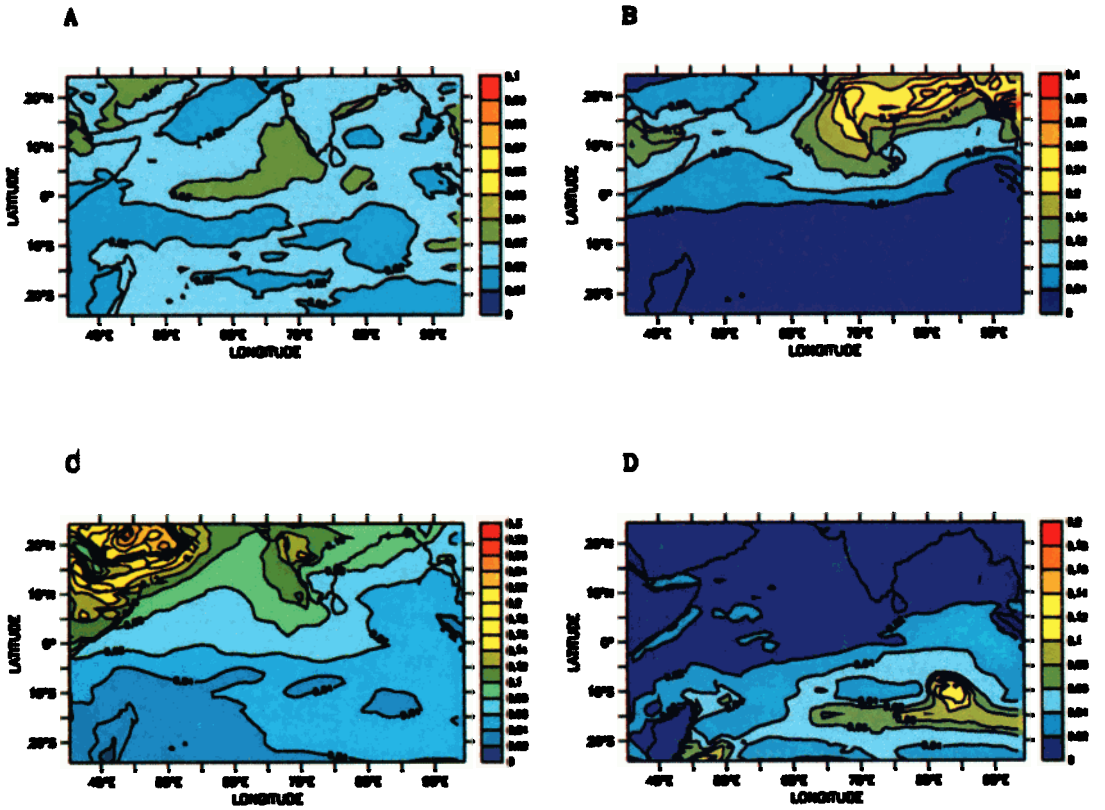

Plate 3. Average aerosol optical depths for each aerosol species for March 1–14, 1999, from the standard integration: (a) sulfate, (b) black and organic carbon, (c) mineral dust, and (d) sea salt. AODs are evaluated at λ = 630 nm. Note difference in scales.

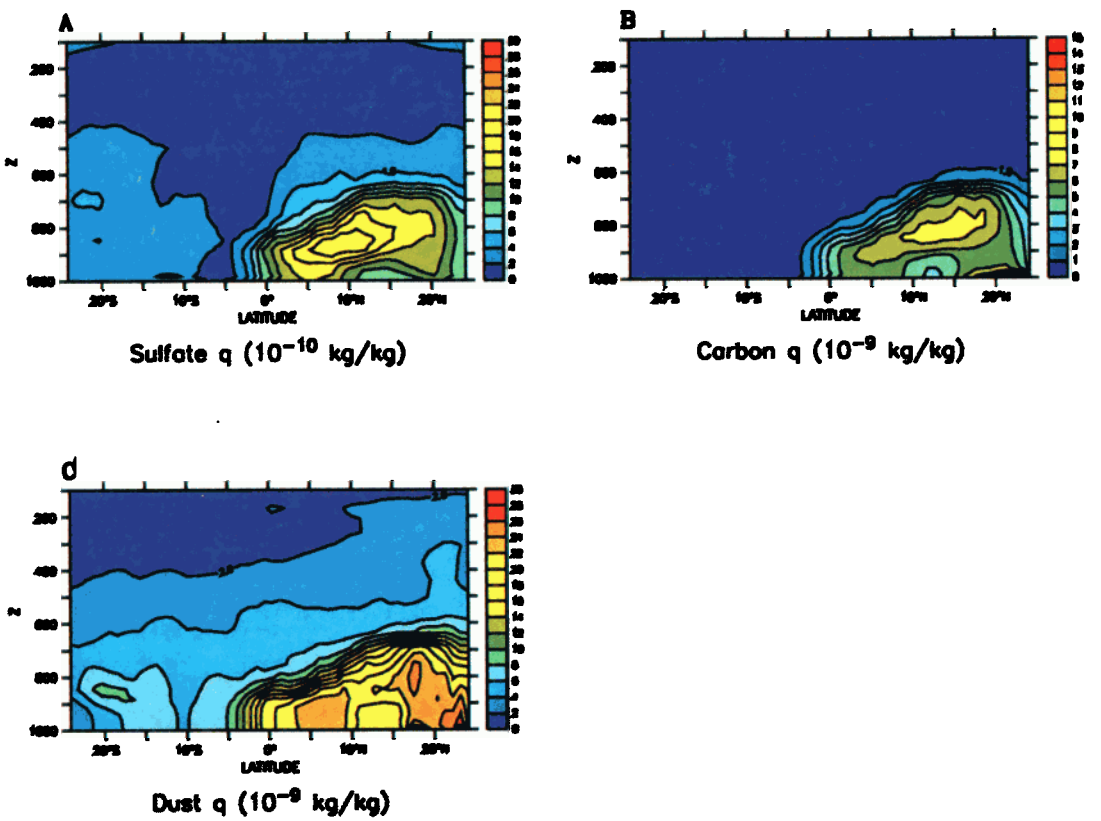

Plate 4. Height-latitude cross sections of aerosol mass-mixing ratios for each aerosol species for March 1–14, 1999, from the standard integration. Profiles have been averaged over 70°–75°E: (a) sulfate, (b) black and organic carbon, and (c) mineral dust. Note difference in scales.

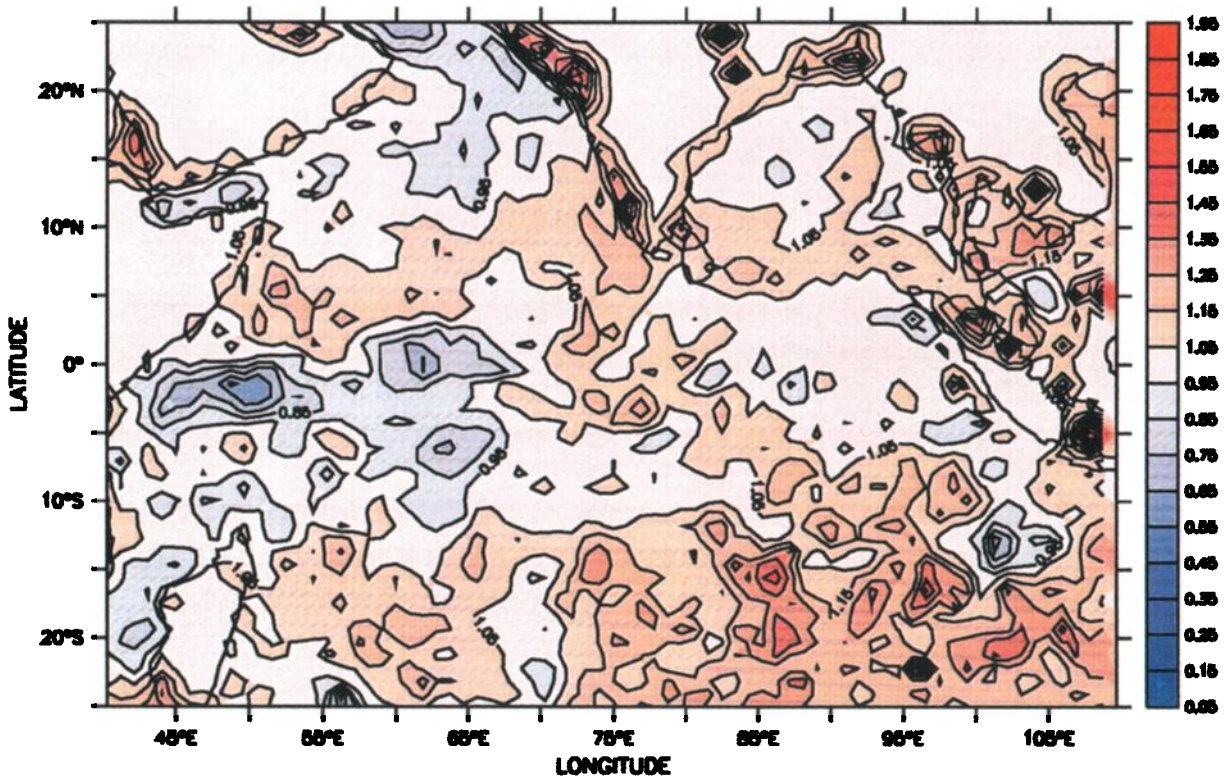

Plate 5. Average multiplicative correction applied to the aerosol optical depth by each assimilation step during the standard simulation of March 1–14, 1999.

representative subset of global models vary by a factor of 3 [*Rasch et al.*, 2000a]. In the same comparison, no model agreed with surface observations of sulfur dioxide and sulfate to within a factor of 2 at all the surface measurement sites. The skill of the models in reproducing the observations is expected to improve with better estimates of emissions, more realistic representations of aerosol chemistry, and more accurate meteorological fields.

In this paper, we suggest that assimilation of aerosol observations may provide a new mechanism for improving the skill of aerosol transport models. Our study is motivated by the success of recent efforts to assimilate measurements of tropospheric and stratospheric trace gases into chemical transport models [*Austin*, 1992; *Fisher and Lary*, 1995; *Elbern et al.*, 1997; *Elbern and Schmidt*, 1999]. A system for forecasting aerosol optical depth (AOD) has been developed by coupling a chemical transport model with a system for assimilating satellite retrievals of AOD. This system was used to forecast aerosol distributions for operational planning during the Indian Ocean Experiment (INDOEX). The system could be readily applied to assist in deployment of measurement platforms in other field programs. The same system is being used to produce four-dimensional gridded aerosol products, or aerosol analyses, analogous to meteorological analyses from operational centers.

Assimilation is one of several methods for improving the fidelity of the model to observations. We should stress, however, that we do not view assimilation as a substitute for improvements in the aerosol source characterization and physical parameterizations. In addition, the assimilation of aerosols is a relatively complex problem because of the multiplicity of aerosol species, uncertainties in the retrieval of aerosol physical and microphysical properties, and uncertainties in the forward models needed to relate the modeled aerosols to the retrievals. Further refinements will require very detailed characterization of the errors in the modeled aerosol distributions and better understanding of the uncertainties in aerosol optical models. The system discussed in this paper should be regarded as a preliminary aerosol assimilation. In the future, assimilation could serve as a powerful diagnostic tool for characterizing errors in the model physics through careful analysis of the corrections applied by assimilation. A major reason for introducing assimilation into an aerosol model is to improve the skill of the model in forecasting short-term variability (less than 1 week) in the spatial distribution of aerosols far from the source regions. Few chemical transport models have been designed with this requirement in mind. In fact, many CTMs demonstrate only modest skill in reproducing monthly variations of important aerosol species.

The system is described in detail in the present paper, and the first aerosol analysis for the INDOEX region is discussed in an accompanying study [*Rasch et al.*, this issue]. The model and assimilation components are described in section 2. The satellite, boundary, and meteorological data sets are discussed in section 3. The application of the system in INDOEX and a brief description of the INDOEX field experiment are contained in section 4. There are significant uncertainties in model parameters governing the action of the assimilation and the estimation of aerosol optical properties. The sensitivity of the aerosol analysis to variations in these parameters is evaluated in section 5. The possible extension of the system to assimilate

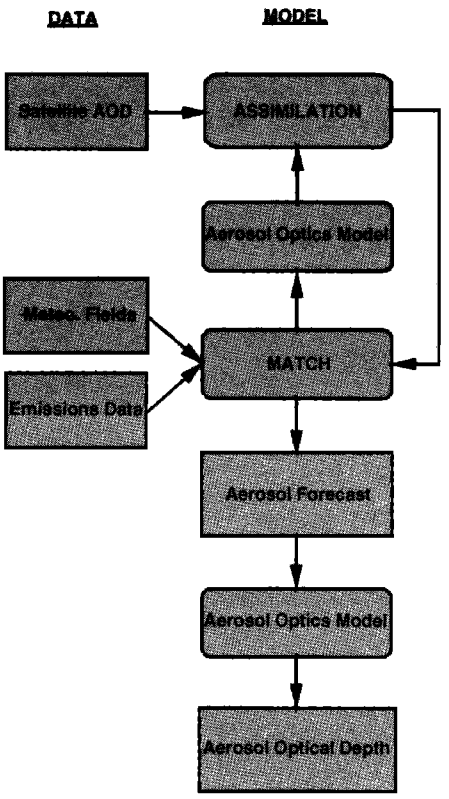

Figure 1. Components of the aerosol analysis system combining an assimilation package and a chemical transport model. The model components are described in section 2, and the input data are described in section 3.

other types of observations is discussed in section 6. Conclusions and future work are presented in section 7.

2. Description of the Model

2.1. Overview

The system used to simulate aerosols combines a chemical transport model together with an assimilation of satellite aerosol retrievals. The model diagnoses sea salt aerosols and predicts sulfate, mineral dust, and carbonaceous aerosols. The evolution of the aerosol field is driven by meteorological fields from an operational forecast center. The model integration proceeds until the model time step matches the time of a satellite overpass and corresponding aerosol retrieval. The total column aerosol optical depth is estimated from the model aerosol fields. The model state is then adjusted to minimize differences between the simulated AOD and satellite retrievals of AOD consistent with the uncertainties in the model and observations [*Lorenc*, 1986]. This process is illustrated in Figure 1. The model then proceeds with the integration until the next assimilation.

2.2. Simulated Fields

Aerosols comprised of sulfate, mineral dust, sea salt, black carbon, and organic carbon components are simulated by the model. At present, heterogeneous aerosols are not included, and all aerosols are treated as external mixtures. In addition, tagged ^{222}Radon from Africa, India, southeast Asia, and Arabia is used to monitor the recent origin of air parcels in the INDOEX region [*Rasch et al.*, this issue].

Sulfate is represented with a single mass-mixing ratio. The formulation of the sulfur cycle is described by *Barth et al.* [2000] and *Rasch et al.* [2000b]. Sulfate is produced through the oxidation of its precursors DMS and SO_2. It is removed by wet and dry deposition processes. The emissions inventory for SO_2 is from *Benkovitz et al.* [1996]. This inventory is based on conditions for 1985, but emissions of SO_2 have changed substantially between 1985 and 1999 in many areas including the Indian subcontinent. The sensitivity of the aerosol distribution to substitution of an inventory for 1999 (S. J. Smith et al., unpublished manuscript, 1999) is discussed by *Rasch et al.* [this issue].

The methodology for mineral dust is based upon the approach of *Tegen and Fung* [1994] with modifications to the soil mobilization to improve agreement with the Nimbus 7 absorptive-aerosol index from *Herman et al.* [1997]. The dust is resolved into four size classes for effective radii between 0.01–1 μm, 1–10 μm, 10–20 μm, and 20–50 μm. Dust is removed from the atmosphere by wet and dry deposition. The coagulation of dust to form larger dust particles is not included in the parameterization. Since estimates of soil moisture are not available from the NCEP aviation analyses used for INDOEX (section 3.3), the soil mobilization is modified using a leaf-area index adapted from the National Center for Atmospheric Research (NCAR) land-surface model (LSM) [*Bonan*, 1996].

In the current implementation, vertical profiles of sea-salt mass are diagnosed from the 10m wind speed using the empirical approach of *Blanchard and Woodcock* [1980]. Between the surface and 300 m, the sea salt concentration $s(z)$ in units of $\mu g/m^3$ is given by

$$s(z) = 5(6.3 \times 10^{-6} z)^{(0.21-0.39 \log_{10} U_{10})}, \quad (1)$$

where z is the height above sea level in meters and U_{10} is the 10-m wind speed (m/s). Above 300 m, the profile decreases exponentially with a 500-m scale height.

The carbonaceous aerosols include black and organic carbon aerosols. These aerosols result from biomass burning [*Liousse et al.*, 1997], fossil fuel burning [*Penner et al.*, 1993], and a source of natural organic aerosols resulting from terpene emissions (J. Penner, personal communication, 1999). The carbonaceous aerosols are assumed to be emitted in a hydrophobic form [*Cooke and Wilson*, 1996]. These aerosols age rapidly with a 1.2 day e-folding time to a hydrophilic form which is subject to wet deposition. This time-scale is intermediate between those used by *Cooke and Wilson* [1996] and *Liousse et al.* [1997] and is adjusted to yield better agreement with measured carbon concentrations. In the current implementation the carbonaceous aerosols are not resolved into size bins.

2.3. Chemical Transport Model

The assimilation system is based upon the Model of Atmospheric Transport and Chemistry (MATCH, version 3.3) [*Rasch et al.*, 1997]. (The code is available from the MATCH website ftp://ftp.cgd.ucar.edu/cms/match.) For INDOEX, MATCH is run in "diagnosed" mode [*Rasch et al.*, 1997]. In "archival" mode all the fields required for integration are available from an external source which is typically a GCM. However, some of the required fields are missing from the NCEP analysis and standard operational forecasts, for example, the vertical convective mass fluxes and three-dimensional precipi-

Table 1. Physical and Optical Properties for Mineral Dust Aerosols

Size, μm	v_g,[a] cm/s	v_t,[b] cm/s	r_g,[c] μm	ln σ_g[d]	χ,[e] m²/g
0.01–1	0.02	0.03	0.4	0.7884	1.303
1–10	1.42	0.50	2.0	0.7884	0.124
10–20	8.39	7.00	15.0	0.7884	0.040
20–50	38.87	25.00	25.0	0.7884	0.017

[a]Gravitational settling velocity.
[b]Turbulent deposition velocity.
[c]Geometric mean radius.
[d]Width of lognormal distribution.
[e]Optical extinction at λ = 630 nm.

tation rates. In diagnosed mode, physical parameterizations are used to derive the missing fields from the input data. The fields from the meteorological analyses are linearly interpolated in time to the current time step of the model. The time step is set to 30 min except for the sulfur package, which is integrated with a subcycle time step of 2 min [*Barth et al.*, 2000]. In each 30-min time step the input data are interpolated, the resolved-scale advection is computed and then the physics and chemistry parameterizations are executed. The assimilation of aerosol observations (section 2.4) is performed after the parameterizations. The assimilation in its current form is equivalent to a three-dimensional source or sink for aerosols, although it is not a dominant term in the aerosol mass budget [*Rasch et al.*, this issue].

At each time step, sulfur, carbon, mineral dust, and radon species undergo transport by resolved scale wind fields, subgrid-scale convective and turbulent transport, chemical transformation, and wet and dry deposition processes. More detailed discussion of these processes can be found in the works of *Rasch et al.* [2000b] and *Barth et al.* [2000].

A prescribed dry deposition velocity is used for the sulfate, hydrophilic, and hydrophobic carbon. The settling velocity for sulfate is 0.2 cm/s. The prescribed velocity for carbon is 0.1 cm/s [*Cooke and Wilson*, 1996; *Liousse et al.*, 1997]. The dry deposition of dust includes gravitational settling and turbulent deposition from the lowest layer to the surface. The settling velocities and turbulent deposition velocities for the four classes of dust are shown in Table 1 [*Seinfeld and Pandis*, 1997, p. 971]. The prescription of a single constant deposition velocity for each species was adopted because it is computationally inexpensive and it does not require that critical fields (e.g., land-surface type) be available at the resolution of the NCEP aviation analysis (section 3.3). This formulation also does not require that additional fields, for example, surface insolation, be available in the operational real-time analysis. In future versions of the model the deposition of sulfate and possibly other species will be computed using a resistance in series approach [*Wesely and Hicks*, 2000].

The aerosols are affected by the representation of the hydrological cycle through several processes including the scavenging of aerosols by precipitation, the aqueous-phase reactions affecting sulfate distributions [*Barth et al.*, 2000], and the hygroscopic growth of the aerosols. Cloud amount is diagnosed from humidity, vertical motion, static stability, and precipitation using the same scheme employed in CCM3 [*Kiehl et al.*, 1998]. The condensed water in the clouds evolves following a prognostic cloud-water parameterization developed by *Rasch and Kristjánsson* [1998]. The liquid and ice water in cloudy regions are affected by condensation, evaporation, precipitation, and subgrid transport. The amount of precipitation and condensation are the primary inputs to the parameterizations of wet scavenging of soluble gases and aerosols. The wet deposition process is identical for sulfate and hydrophilic carbon aerosols. The three-dimensional production of precipitation and condensate is derived internally by the model run in the diagnosed mode since it is not generally available from meteorological analyses. The impact of inaccuracies in the diagnosed precipitation on wet deposition is evaluated by *Rasch et al.* [1997].

2.4. Assimilation Package

The assimilation procedure is based upon the optimal interpolation approach commonly used for meteorological applications [*Lorenc*, 1986]. The procedure for aerosols is adapted from an assimilation package developed for modeling trace gases in the atmosphere [*Levelt et al.*, 1998; *Lamarque et al.*, 1999]. The procedure modifies modeled fields to match observations in a manner consistent with uncertainties in the modeled and observed quantities. In this application the observations are retrievals of AOD denoted τ_o. The corresponding modeled values of AOD are denoted τ_m and are given by an integral over pressure

$$\tau_m = g^{-1} \int_0^{p_s} \sum_i \chi_i(p) q_i(p)\, dp. \tag{2}$$

Here i is an index for aerosol species, χ_i is the optical extinction for each species, q_i is the corresponding aerosol mixing ratio, g is gravitational acceleration, and p_s is the surface pressure. The dependence on lateral coordinates has been omitted for simplicity. The value τ_m can be represented by a sum over the layers in the vertical grid:

$$\tau_m = \sum_k \tau_m(k),$$

$$\tau_m(k) = g^{-1} \int_{p_k}^{p_{k+1}} \sum_i \chi_i(p) q_i(p)\, dp. \tag{3}$$

The values of $\tau_m(k)$ immediately after assimilation are given by

$$\boldsymbol{\tau}'_m = \boldsymbol{\tau}_m + \mathbf{K}(\boldsymbol{\tau}_o - \mathbf{H}\boldsymbol{\tau}_m), \tag{4}$$

where $\mathbf{H}$ is a linear operator for interpolation from the model grid to the locations of the observations, and $\mathbf{K}$ is the Kalman gain matrix. The collection of satellite retrievals for various locations is represented by $\boldsymbol{\tau}_o$, and the three-dimensional grid of values for $\tau_m(k)$ is represented by $\boldsymbol{\tau}_m$. Since we average the high-resolution satellite observations onto the same grid used by MATCH, the horizontal component of $\mathbf{H}$ is the identity matrix $\mathbf{I}$. From (3) the vertical component of $\mathbf{H}$ is a vector with 1 as each component. Assuming that the errors are Gaussian distributed and that the errors in model and data are uncorrelated, then $\mathbf{K}$ is given by

$$\mathbf{K} = \mathbf{B}\mathbf{H}^T(\mathbf{H}\mathbf{B}\mathbf{H}^T + \mathbf{O})^{-1}. \tag{5}$$

Covariances of the analyzed (assimilated) and observed fields are represented by matrices $\mathbf{B}$ and $\mathbf{O}$, respectively. The on-diagonal elements are the root-mean-square (RMS) errors in the model and data at a single point, and the off-diagonal

Table 2. Free Parameters in the Assimilation Process

Variable	Symbol	Value
Fractional error in model τ	f_m	0.5
Fractional error in observational τ	f_o	0.2
Minimum RMS uncertainty in model τ	ε_m	0.0
Minimum RMS uncertainty in obs. τ	ε_o	0.04
Horizontal correlation length for errors in obs. τ	ℓ_{ox}	0 km[a]
Horizontal correlation length for errors in model	ℓ_{mx}	100 km
Vertical correlation length for errors in model	ℓ_{mz}	1 km

[a]Horizontal correlation lengths for the data are set to 0 km for nadir-pointing satellite instruments. Errors in the satellite retrievals for adjacent pixels are assumed to be completely decorrelated to first approximation.

elements give the error covariances between two locations. If the observational errors are negligible compared to the model uncertainties, then $\mathbf{K} = \mathbf{H}^{-1}$ and (4) yields $\boldsymbol{\tau}'_m = \mathbf{H}^{-1}\boldsymbol{\tau}_o$. In this limit the assimilation procedure forces the model estimates to agree with the observations. In our application the observational errors cannot be neglected, and the procedure gives a "softer" adjustment to the model.

The errors in the satellite data are assumed to be uncorrelated at the horizonal length scale of the model. Therefore the observational error matrix $\mathbf{O}$ is diagonal. The errors in individual estimates of τ_o include a minimum RMS error $\varepsilon_o = 0.04$ and a fractional uncertainty in the estimate of $f_o = 0.2$ [*Stowe et al.*, 1997]. Therefore $\mathbf{O}$ is given by

$$\mathbf{O} = [(f_o\tau_o)^2 + (\varepsilon_o)^2]\mathbf{I}. \tag{6}$$

The expression for the model covariance matrix has the form:

$$\mathbf{B}(d_x, d_z) = [(f_m\tau_m)^2 + (\varepsilon_m)^2] \exp\left[\frac{-d_x^2}{2\ell_{mx}^2}\right] \exp\left[\frac{-d_z^2}{2\ell_{mz}^2}\right]. \tag{7}$$

Here d_x is the horizontal distance between two model grid points, and ℓ_{mx} is the horizontal correlation length-scale for errors in the model fields. The corresponding vertical distance and vertical correlation length-scale are d_z and ℓ_{mz}, respectively. The fractional uncertainty and minimum RMS error in the model estimates of AOD are denoted f_m and ε_m, respectively.

The complete list of tunable parameters in the assimilation scheme is given in Table 2, which includes all the constants in (6) and (7) for the observational and model covariance matrices. In this initial study of aerosol assimilation the values for most of these parameters have not been determined from quantitative error analysis and are subject to large uncertainties. As noted above, the fractional and minimum errors in the satellite retrievals (f_o and ε_o, respectively) are taken from *Stowe et al.* [1997]. We have assumed that the minimum model error (ε_m) is identically 0 and that the fractional model error (f_m) is 50%. On the basis of comparison of sulfate concentrations from MATCH and surface observations [*Rasch et al.*, 2000a] the error estimates for the model are probably conservative. The horizontal correlation length (ℓ_{mx}) is set to 100 km. This value is qualitatively consistent with preliminary analysis of data from the Lidar In-Space Technology Experiment (LITE) [*Winker et al.*, 1996]. The LITE data suggest that aerosol fields have a horizontal correlation length scale of ~200 km (D. M. Winker and R. J. Charlson, personal communication, 1999). Since the model grid spacing is ~100 km at the equator, the value chosen for ℓ_{mx} implies that model errors decorrelate rapidly with separation on the model grid. The vertical correlation length for errors in the model (ℓ_{mz}) is assumed to be 1 km. The sensitivity of the simulation to changes in these a priori values is examined in section 5.4.

The assimilation is used to apply a correction to the model at each model time step immediately following a satellite overpass (section 3.2). Because of the short duration of an individual satellite overpass and the rapid evolution of the aerosol field, the corrections required to obtain $\boldsymbol{\tau}'_m$ from $\boldsymbol{\tau}_m$ are applied only at the time step closest to the time of an overpass. The duration of each satellite overflight of the INDOEX region is generally <20 min, or 66% of the model time step.

Since the model estimate of $\boldsymbol{\tau}_m$ includes contributions from four different aerosol species, the assimilation problem is underdetermined. It is not clear a priori how to partition the correction from $\boldsymbol{\tau}_m$ to $\boldsymbol{\tau}'_m$ among the various species. The indeterminacy can be reduced once the in situ observations of chemical speciation or estimates of multispectral aerosol optical depth become available from INDOEX surface sites (section 6). However, an ad hoc assumption is required for partitioning the correction when the observations include only total AOD. Since the sea salt aerosols are diagnosed rather than evolved, the model values τ_s for sea salt AOD are held fixed during the assimilation procedure. The difference $\hat{\tau}_o = \tau_o - \tau_s$ is assumed to be contributed by a combination of sulfate, dust, and carbonaceous aerosols. The assimilation is then applied to $\hat{\tau}_m = \tau_m - \tau_s$ to correct the non sea salt aerosols in the model. At each model level the mass mixing ratios for sulfate, dust, and carbonaceous aerosols are multiplied by the ratios of $\hat{\tau}'_m(k)/\hat{\tau}_m(k)$. Since AOD is proportional to the mixing ratios, this adjustment guarantees that the modeled AOD equals $\hat{\tau}'_m$. At present, there is insufficient information on the errors in each individual species to justify the use of separate multipliers. If $\tau_s > \tau_m$, no correction is applied. This situation occurs infrequently in the northern Indian Ocean where the sea salt is a relatively minor component of the total optical depth [*Rasch et al.*, this issue].

2.5. Aerosol Optics

The assimilation of AOD requires optical extinction coefficients for each of the aerosol species (equation (2)). The coefficients are functions of the size distribution of the aerosols, and the present version of the model does not carry information regarding the size distributions of the sulfate, sea salt, and carbon. Size distributions are prescribed for the sulfate and sea salt to conform with published estimates (described below) of the size parameters and optical properties of these aerosols. Size-resolved sulfate and sea salt aerosols will be implemented in the next version of the model. Sensitivity of the assimilation to the choice of optical extinctions is analyzed in section 5.3.

The optical extinctions can be specified as a product of a prescribed "dry" value and a hygroscopic growth factor that is a function of relative humidity (RH):

$$\chi_i = \chi_i(\mathrm{RH} \ll 1) f_i(\mathrm{RH}). \tag{8}$$

The hygroscopic extinction correction can be significant, e.g., for sulfate aerosols, f_i in visible wavelengths increases from 1.7 to 7.0 as the relative humidity increases from 50 to 90% [*Kiehl et al.*, 2000].

The sulfate optics are taken from *Kiehl et al.* [2000]. The size distribution for the dry sulfate aerosol distribution is assumed to be lognormal, and the effects of hygroscopic growth are computed from the Köhler curve. To a very good approximation, the size distribution of the hydrated aerosol can also be fit to a lognormal distribution. The geometric mean radius r_g, standard deviation σ_g, and optical properties can be expressed as functions of relative humidity. For the assimilation system the sulfate is assumed to be H_2SO_4 with dry size parameters $r_g = 0.05$ μm and $\sigma_g = 2.03$ μm. These properties agree with the characteristics of the maritime sulfate aerosols of *Shettle and Fenn* [1975] and *d'Almeida et al.* [1991].

The sea-salt optics are adapted from *Quinn and Coffman* [1999] following *Haywood and Ramaswamy* [1998]. *Quinn and Coffman* [1999] estimate a mean mass-weighted extinction of 2.5 m^2/g at 70% relative humidity and $\lambda = 550$ nm from several experimental cruises. Their data include measurements from tropical and midlatitude meteorological regimes. The extinction is scaled to other relative humidities using hygroscopic growth factors based on the Köhler curve (S. Dobbie, private communication, 1999). Mie calculations indicate that the extinction at 630 nm, the wavelength of the AVHRR observations (section 3.2), differs from the value at 550 nm by a few percent.

The dust optical properties are derived from Mie theory. The index of refraction used for the dust is appropriate for Saharan dust aerosols [*Patterson*, 1981]. The dust in each size class is distributed according to a lognormal distribution. The size parameters and extinction coefficients for each size class are given in Table 1. No hygroscopic growth factors are applied to the dust extinction coefficients. The AOD of the submicron bin is the dominant contribution to the total dust AOD. The optical properties of the submicron bin follow from assuming that surface area is distributed within the bin according to *Patterson and Gillette* [1977], who found that a lognormal size distribution with $r_g = 0.4$ μm and $\sigma_g = 2.2$ best fits their in situ measurements. *Schulz et al.* [1998] found that a modified version of the "background desert model" size distribution of *Shettle* [1984] with $r_g = 0.3$ μm and $\sigma_g = 2.0$ reproduces observed AOD from long-range transported desert dust aerosol very closely. The *Schulz et al.* [1998] size distribution leads to optical extinctions per unit mass 15% greater than extinctions derived from the *Patterson and Gillette* [1977] size distribution used in this paper. This is an uncertainty of order 15% rather than a systematic bias since dust size distributions during INDOEX may differ significantly from both of these analytic size distributions.

The extinction values for carbonaceous aerosols have the greatest uncertainty. The extinction varies from 2.5 to 12 m^2/g, depending on the chemical and physical properties of the carbonaceous aerosols [*Liousse et al.*, 1996; *Tegen et al.*, 1997]. We use $\chi_C = 9$ m^2/g for both hydrophilic and hydrophobic carbon following *Haywood and Ramaswamy* [1998]. Since the uncertainties in χ_C for the dry carbon are much larger than typical hygroscopic growth factors, no hygroscopic growth is applied to the carbon extinctions. The sensitivity of the simulated aerosol distributions to carbon extinction is discussed in section 5.3. The ad hoc values of χ_C will be replaced with in situ observations from INDOEX once these observations become available (section 6). The optical properties for black and organic carbon are quite different, and different optical properties should be specified for black carbon and hydrophilic and hydrophobic organic carbon [e.g., *Cooke et al.*, 1999].

The aerosol optical models used to construct the satellite retrievals (section 3.2) do not necessarily correspond to the representation of aerosols in MATCH. The satellite retrievals are generally based upon a limited set of characteristic aerosol models, for example the maritime aerosol type of *d'Almeida et al.* [1991]. A CTM can readily generate mixtures of aerosol species with optical properties that do not correspond to any of the characteristic aerosol models. Thus the relationships between aerosol mass and aerosol optical depth in the retrieval and CTM will not be identical. These differences will lead to systematic errors in the corrections applied by the assimilation. In principle, the best solution would be to compute the relationships between aerosol mass, optical depth, and satellite radiances directly from the representation of aerosols in the CTM. This approach has not been adopted in the present version of the assimilation system because of the significant computational cost of the forward radiative transfer calculations. It is possible that future versions of aerosol assimilation could be based upon adjoints of the radiative transfer equations.

3. Description of the Input Data

3.1. Prescription of Aerosol Sources

The model includes sources for sulfur and carbonaceous compounds. The sources for DMS, SO_2, and SO_4^{2-} are described by *Barth et al.* [2000]. Anthropogenic sources of SO_2 and SO_4^{2-} are from the GEIA emissions data set [*Benkovitz et al.*, 1996] and the IPCC emissions data set [*Smith et al.*, 1999]. The emissions are specified both at the surface and 100 m in order to represent low-temperature burning and plumes from high-temperature combustion. The vertical profile of emissions is interpolated onto the lowest two model levels. The emission of DMS is estimated from an inventory of biological sulfur based upon *Kettle et al.* [1999]. Sources of DMS are represented by the subset of biogenic emissions over oceans. The sources for carbonaceous aerosols include contributions from biomass burning [*Liousse et al.*, 1996], fossil fuel combustion [*Penner et al.*, 1993], and natural organics (J. Penner, personal communication, 1999). The database for biomass burning and fossil fuel combustion includes sources for black and organic carbon. The production of natural organics is assumed to comprise 10% of the total emissions of terpene from *Guenther et al.* [1995]. The carbon sources are treated as surface fluxes and are interpolated to T126 resolution with an adjustment proportional to the fraction of land within each grid box that conserves total emissions but restricts emissions to land points.

3.2. Satellite Retrievals of Aerosol Optical Depth

Estimates of column-integrated AOD are derived from imagery from the Advanced Very High Resolution Radiometers (AVHRR) on NOAA 14 using the second-generation Pathfinder aerosol algorithm [*Stowe et al.*, 1997]. The characteristics of the AVHRR data are given by *Kidwell* [1998]. The basis of the Pathfinder algorithm is a precomputed look-up table relating variations in AVHRR visible radiances measured at 630 nm to variations in AOD. The aerosol is assumed to have optical characteristics similar to those of a marine aerosol [*Stowe et al.*, 1997]. Other retrievals have been developed specifically for the heavily polluted conditions in the INDOEX region [e.g., *Rajeev et al.*, 2000], but the new retrievals are not available for use in the assimilation at this time. The Pathfinder method is limited to ocean regions where the surface reflec-

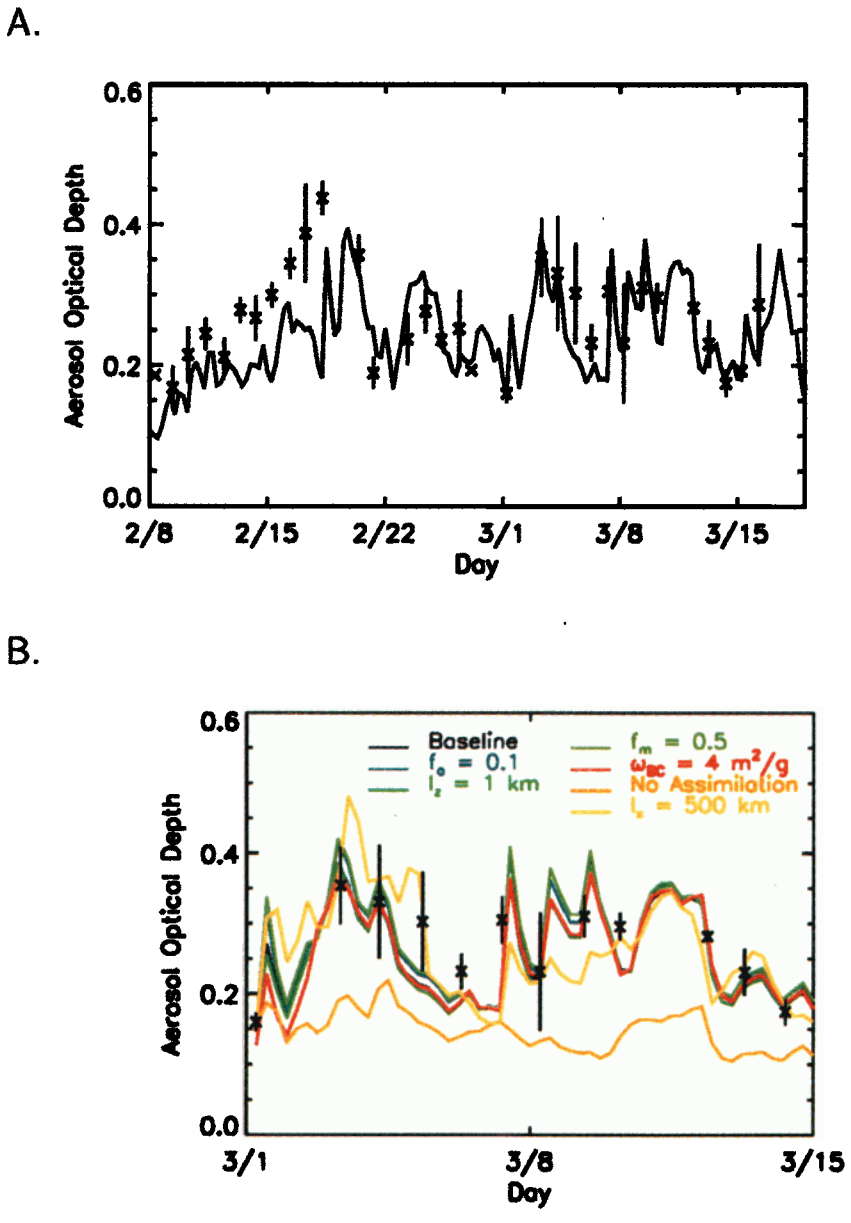

Plate 6. Comparison of daily-mean AOD from the assimilation system (solid lines) and from a Microtops Sun photometer (crosses) [*Satheesh and Ramanathan*, 2000]. The vertical bars represent the RMS differences between instantaneous measurements and the daily means. Sun photometer measurements of direct solar insolation are for λ = 675 nm, and the model AODs are estimated at λ = 630 nm: (a) baseline simulation and (b) sensitivity experiments (section 5) and baseline simulation for March 1–14, 1999.

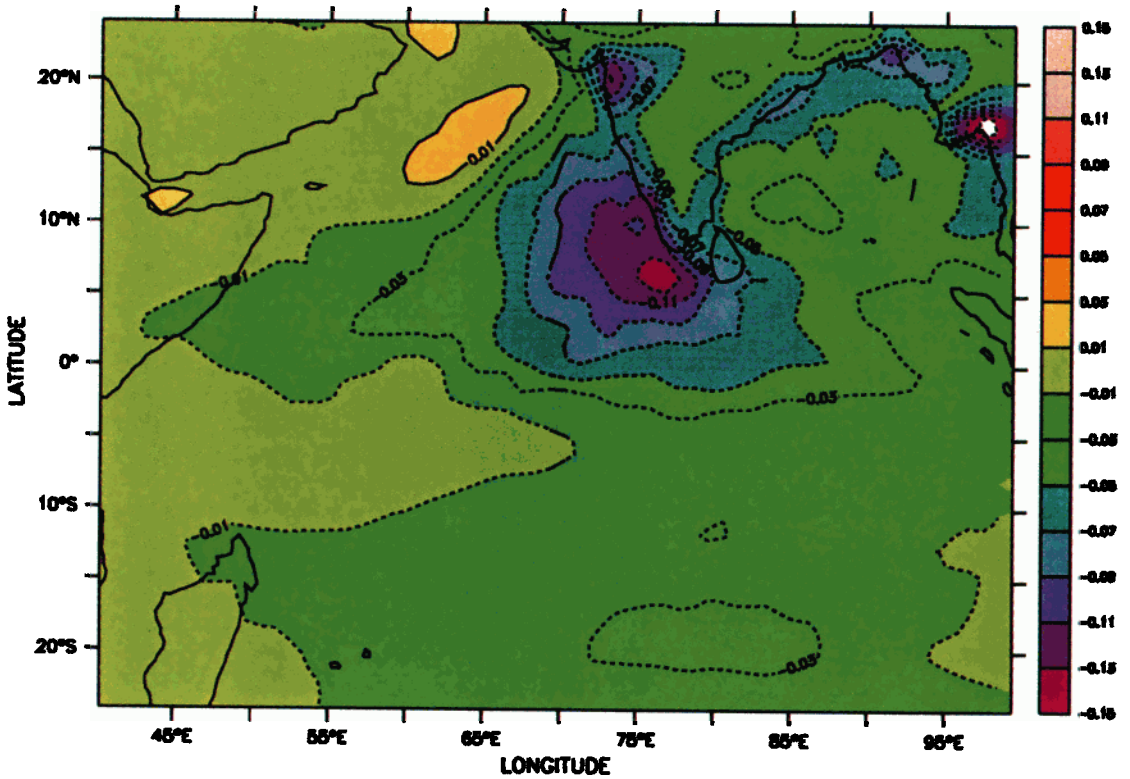

Plate 7. Differences between average aerosol optical depths from the simulation without assimilation and the standard integration. Time period and wavelength are identical to Plate 1.

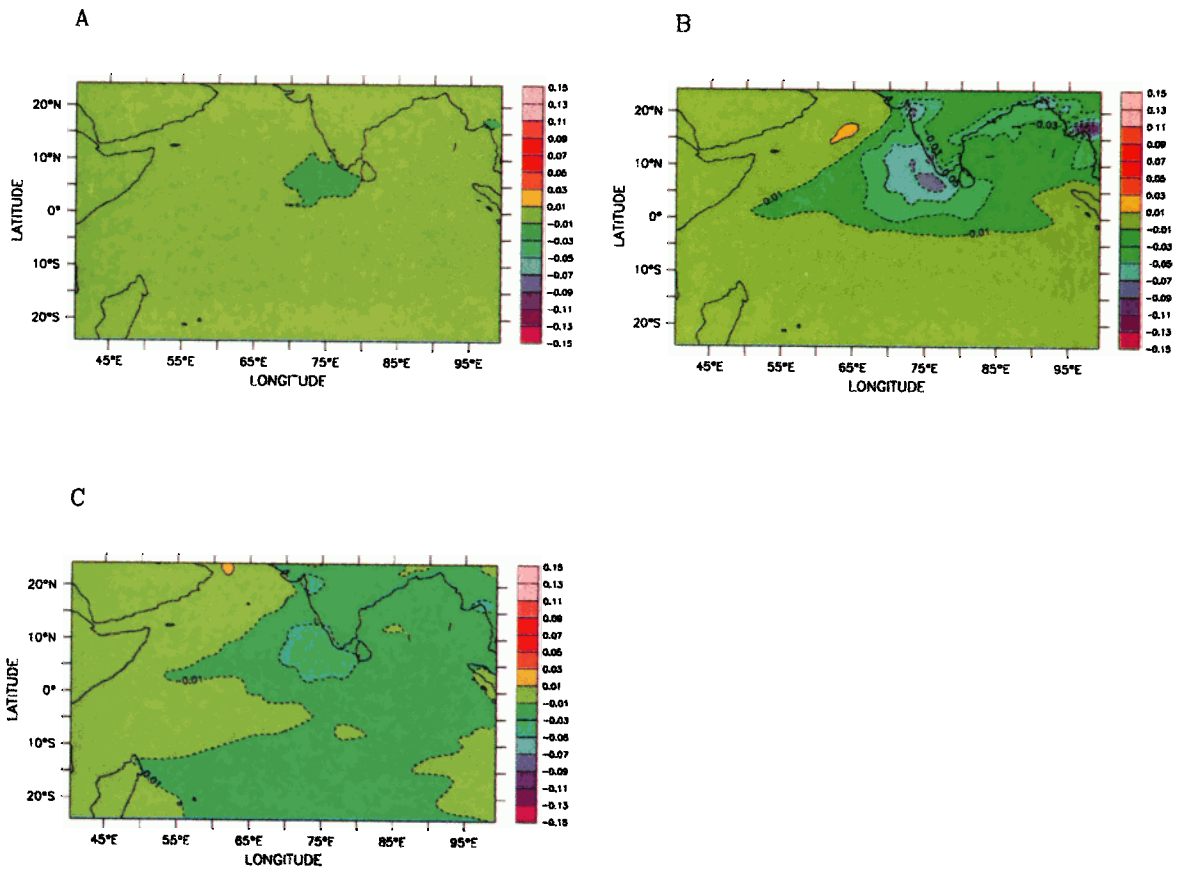

Plate 8. Differences between average aerosol optical depths for each aerosol species from the simulation without assimilation and the standard integration. Time period and wavelength are identical to Plate 3: (a) sulfate, (b) black and organic carbon, and (c) mineral dust.

tivity is a known function of wind-speed (e.g., *Mishchenko and Travis* [1997]) and is close to 0 in the spectral bandpass of the AVHRR instrument. The method is further limited to cloud-free pixels identified using the Clouds from AVHRR (CLAVR) phase-1 cloud-screening algorithm [*Stowe et al.*, 1998]. Thus the assimilation is performed only for cloud-free ocean regions. Errors in, for example, the terrestrial sources for aerosols can be addressed only after the air masses containing these aerosols are advected over the open oceans. However, the assimilation can be readily extended to continental regions using surface-based instruments and the next generation of satellite retrievals (section 7).

The second-generation Pathfinder data set compares favorably with Sun photometer observations [*Stowe et al.*, 1997]. Relative to Sun photometer data from three surface sites, the systematic error is <10%, and the random error is approximately $\sigma_\tau = 0.04$. The Pathfinder group is developing error estimates specifically for dust (L. Stowe, private communication, 1999). Like other aerosol retrieval schemes of its class, the errors in τ from the NOAA Pathfinder algorithm can be large when the optical properties of the observed aerosol depart significantly from the properties adopted in the retrieval [*Mishchenko and Travis*, 1997]. Comparison of satellite retrievals based upon purely scattering optics with estimates of AOD from surface Sun photometers in the INDOEX region indicates that these retrievals underestimate the AOD by ~32% [*Rajeev et al.*, 2000]. Since the optics for maritime aerosols yield nearly conservative scattering at the wavelength of the AVHRR visible radiances, this error estimate may be applicable to the NOAA Pathfinder retrievals in the INDOEX domain. This error estimate has been derived after the development of the original assimilation system based upon the Pathfinder retrieval, and future versions of the system will be based upon more accurate satellite AODs.

Satellite retrievals based upon AVHRR data for the Indian Ocean region are assimilated for INDOEX. The orbit of the NOAA 14 satellite crosses the equator during daylight hours at roughly 1330, which corresponds to 0830 GMT for the INDOEX region. The visible imagery from NOAA 15 is often adversely affected by large solar zenith angles and is not used for aerosol retrievals. Usually, three images from NOAA 14 from afternoon overflights of the INDOEX region are available for assimilation. The time separation between successive images corresponds to the orbital period of ~102 min. Both local area coverage (LAC) imagery with 1.1-km nadir resolution and global area coverage (GAC) imagery, which is subsampled to 3 × 5 km resolution, are used for the INDOEX forecasts. Only data from the antisolar side of the visible imagery is used in the retrievals to avoid problems with Sun glint [*Stowe et al.*, 1997]. Images from successive orbits are separated by ~26° of longitude. The restriction to the antisolar portion of each image yields satellite maps of aerosols from each overpass that span the meridional extent of the INDOEX region and extend ~13° in longitude.

3.3. Meteorological Fields

For INDOEX the assimilation system is integrated using meteorological fields in the aviation forecasts and analyses from the National Center for Environmental Prediction (NCEP) [*Caplan et al.*, 1997; *Parrish et al.*, 1997]. The spectral truncation of the NCEP products is T126, which is equivalent to a horizontal resolution of ~0.9° on the equator. There are 384 longitude and 192 latitude intervals on the Gaussian grid.

Table 3. Meteorological Variables Required to Run CTM

Variable	Units	Module[a]
Zonal wind	m/s	MATCH
Meridional wind	m/s	MATCH
Surface pressure	Pa	MATCH
Orography (land/ocean) flag	...	MATCH
Surface geopotential	m^2/s^2	MATCH
Temperature	K	MATCH
Specific humidity	kg/kg	MATCH
Surface temperature	K	MATCH
Zonal surface stress	N/m^2	MATCH
Meridional surface stress	N/m^2	MATCH
Surface sensible heat flux	W/m^2	MATCH
Surface water vapor flux	$kg/m^2/s$	MATCH
Downward solar flux at surface	W/m^2	DD/SM
Water equivalent snow depth	m	DD/SM
Soil volumetric water content at surface	m^3/m^3	DD/SM

[a]MATCH is Model of Atmospheric Transport and Chemistry, and DD/SM stands for dry deposition/soil mobilization parameterization.

The products are vertically discretized on 28 sigma levels [*Kalnay et al.*, 1996]. The variables required to integrate the assimilation system are listed in Table 3. As noted in section 2.3, the three-dimensional properties of the cloud and precipitation fields are required to estimate the in-cloud oxidation of SO_2 and the wet-deposition rates. These fields are not available from operational forecast center products. For this reason, the three-dimensional fields are reconstructed within MATCH using the physical parameterizations from the NCAR CCM3 [*Rasch et al.*, 1997; *Barth et al.*, 2000].

4. Application to INDOEX

4.1. Description of INDOEX Intensive Field Phase

The INDOEX Intensive Field Phase (IFP) was conducted between February 1 and April 1, 1999. The principal scientific goals of INDOEX are to improve understanding of aerosols, clouds and chemistry-climate interactions, and to use the data collected during INDOEX for evaluation of the representation of aerosols in GCMs and chemical transport models [*Ramanathan et al.*, 1996]. The supporting scientific objectives are to reassess the significance of sulfates and other continental aerosols for global radiative forcing and to assess the role of the Intertropical Convergence Zone (ITCZ) in the transport of trace species and pollutants.

The Indian Ocean has been selected for measuring the transport, properties, and radiative effects of aerosols because of the favorable meteorological conditions during the winter monsoon. During the winter monsoon the prevailing low-level winds in the northern Indian Ocean are northeasterly while the prevailing low-level winds in the southern Indian ocean are southerly [*Krishnamurti et al.*, 1997a]. These wind patterns transport continental and anthropogenic aerosols from India and Arabia over large areas of the Arabian sea and from India and southeast Asia over large areas of the Bay of Bengal [*Krishnamurti et al.*, 1997b]. The polluted air is advected as far south as the ITCZ. The convergence of unpolluted air from the southern Indian ocean and polluted air from the northern Indian ocean should establish a large gradient in aerosol loading close to the ITCZ. The expected geographic gradients in pollutants have been confirmed during pre-INDOEX ship experiments [*Rhoads et al.*, 1997; *Jayaraman et al.*, 1998]. One of

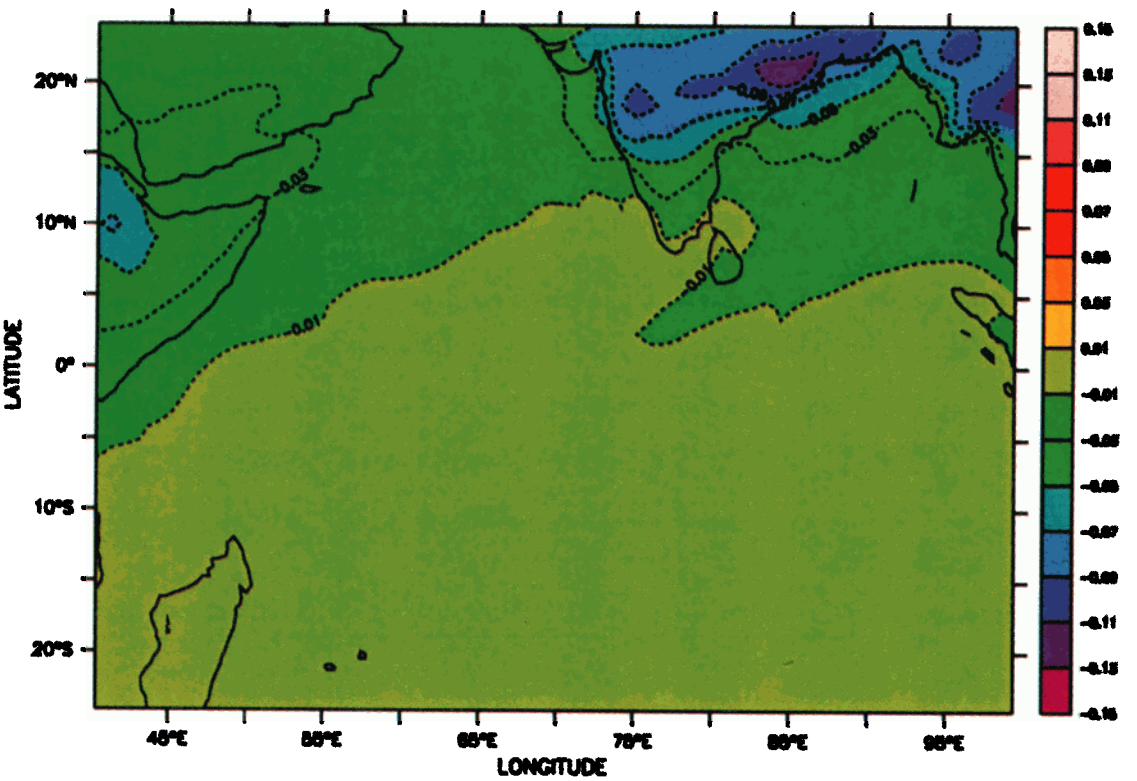

Plate 9. Differences between average aerosol optical depths from the simulation with $\chi_C = 4$ m^2/g and the standard integration with $\chi_C = 9$ m^2/g. Time period and wavelength are identical to Plate 1.

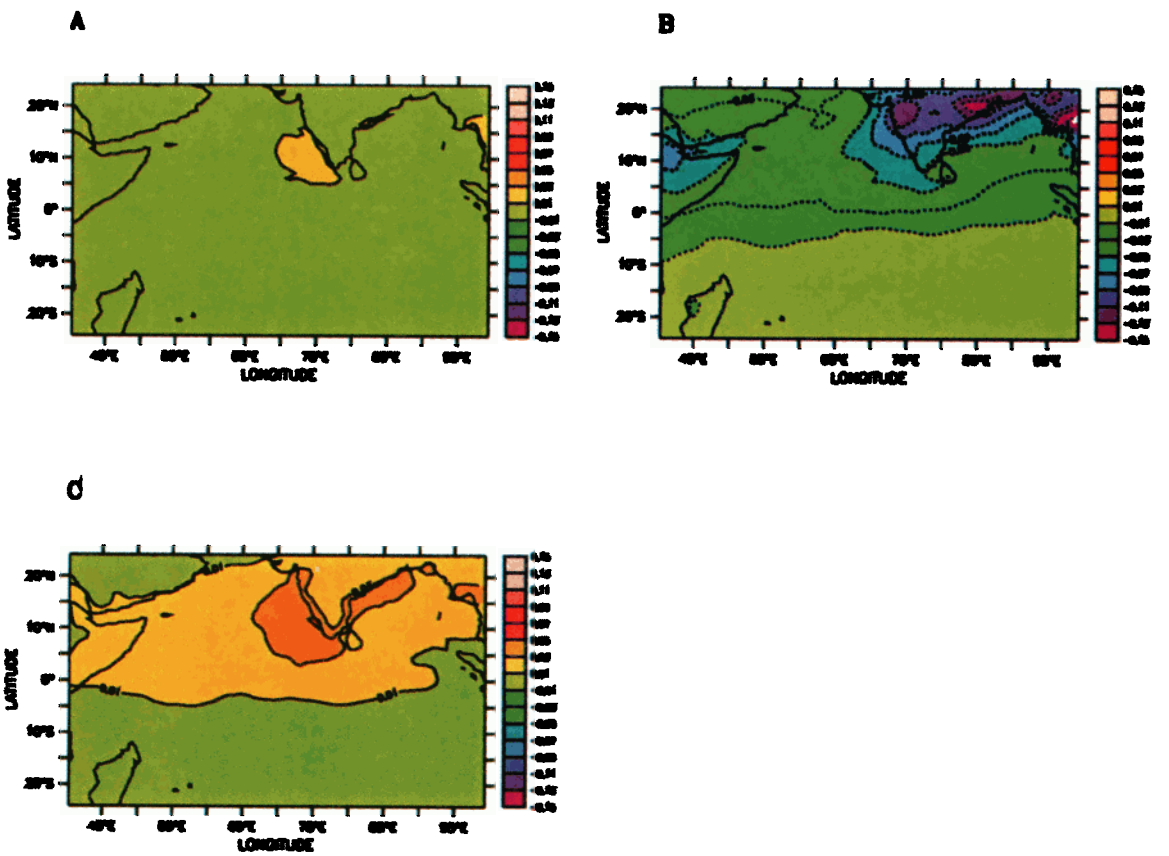

Plate 10. Differences between average aerosol optical depths for each aerosol species from the simulation with $\chi_C = 4$ m^2/g and the standard integration with $\chi_C = 9$ m^2/g. Time period and wavelength are identical to Plate 3: (a) sulfate, (b) black and organic carbon, and (c) mineral dust.

the objectives of the IFP is to sample aerosol distributions and properties across this gradient.

During the IFP, measurements were collected from ships, surface sites, aircraft, constant-level drifting balloons, and satellites in support of the INDOEX objectives. Some of these measurements will be used to improve the CTM/assimilation system (section 6). The aerosol forecasts were used to guide the deployment of the NOAA research vessel R/V *Ron Brown* and the NCAR C-130. The R/V *Ron Brown* carried instrumentation to characterize the chemistry of the boundary layer, the chemical and physical properties of the boundary layer aerosols, and the impact of aerosols on the spectral and broadband solar radiation reaching the ocean surface. The C-130 carried instrumentation to gather similar data in the troposphere. In addition, measurements of cloud physical properties, the upwelling visible and near-infrared radiance field, and vertical lidar profiles of aerosols were collected from the C-130. The C-130 missions were designed to characterize the direct and indirect forcing of aerosols, the gradients and vertical profiles of aerosol properties and radiative forcing, and the consistency of the aircraft measurements with ship and surface-based data.

4.2. Construction of the Aerosol Forecasts

In order to help plan the research missions of the C-130, the CTM was used to generate 24- and 48-hour forecasts of the total AOD at 630 nm and the distribution of tagged ^{222}Radon. The validation time of the forecasts was 6 GMT, which corresponds to 1100 LT at the Maldives. The time line for a typical 24-hour forecast is shown in Figure 2. The aerosol forecast consisted of a two-stage process. During the first stage the model was run using a combination of alternating analysis and forecast fields from the NCEP aviation analysis. The AVHRR derived estimates of AOD were assimilated at the time steps matching the satellite observation times. During the second stage, only NCEP forecast fields were used, and no satellite data was available. Thus the simulated aerosol field were constrained as strongly as possible during the first stage by observations of the meteorological fields and the satellite retrievals. During the second stage, no observations were available, and the simulation was expected to depart more strongly from an accurate forecast.

The initial time step of each run corresponded to 0 GMT 2 days before the validation time, and therefore the 24-hour forecasts required integrations over 54 hours of model time. The forecasts were initialized with the instantaneous model state from a previous integration. During the initial 18-hour assimilation phase the fields from the 6-hourly analyses are alternated with forecast fields for the 3-hour midpoints between adjacent analyses to give 3-hourly temporal resolution. Satellite retrievals of AOD were assimilated during this phase (section 3.2). During the subsequent 36-hour forecast phase the 3-hourly forecast fields are input to the model. Since MATCH is integrated in a global mode, the global NCEP fields are ingested. NCEP provided the fields within ~6 hours after the validation time for the analyses.

This schedule did not permit the incorporation of the most recent meteorological analysis and satellite retrievals from the day before the validation time of the aerosol forecast. The schedule was dictated by severe limitations on communication between the INDOEX operations center in Male, NCEP, and the system generating the aerosol forecast at NCAR. The NCEP fields were used in INDOEX because they are readily available in near real-time.

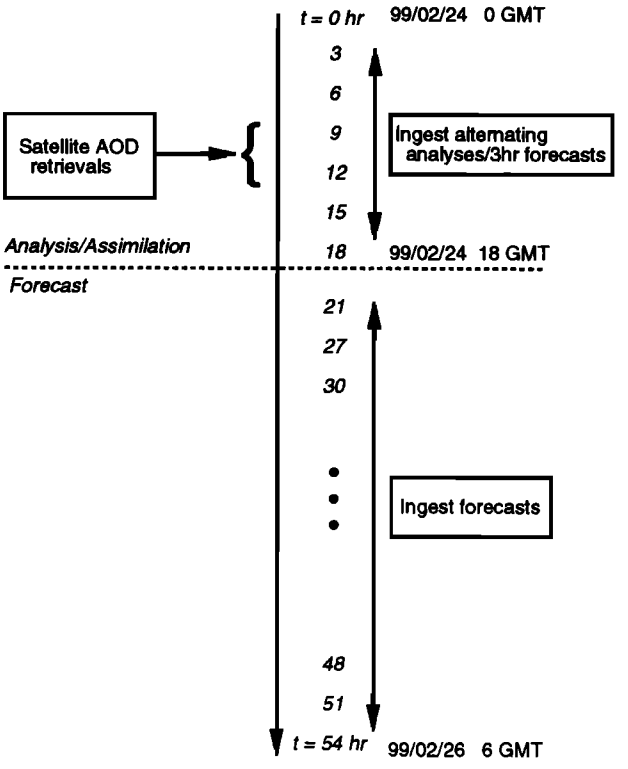

Figure 2. Timeline for production of a 24-hour aerosol forecast during INDOEX. In this example, the forecast is produced and transmitted to the INDOEX operations site by 6 GMT February 25, 1999, 24 hours before the validation time of the forecast. The system is initiated using the instantaneous state of the model from a previous integration. The first 18 hours of simulation is based upon NCEP meteorological analysis fields and assimilation of NOAA Pathfinder aerosol retrievals. At the end of 18 hours the integration continues for 36 additional hours using NCEP meteorological forecasts.

5. Sensitivity Experiments

The aerosol analysis produced by the assimilation system depends on physical parameterizations in the CTM, the input data sets, and the operation of the assimilation scheme. The input data sets include the meteorological fields, the source distribution of aerosol precursors, and the satellite retrievals of aerosol optical depth. Detailed examination of the sensitivity of the analysis to changes in each of these components is beyond the scope of this study. However, initial sensitivity studies have been conducted to determine which components are the most critical to the simulated aerosol distributions.

The studies are integrations of the model for March 1–14, 1999. The initial condition for each integration is the instantaneous state of the basic model integration for INDOEX at 0000 GMT March 1, 1999. The integration of the basic model is driven using the NCEP T126 meteorological analysis fields alternating with intermediate 3-hour forecast fields. The sensitivity studies are limited to a 2-week time period in order to reduce the computational cost and permit more studies to be conducted. The simulation of the aerosol fields in the standard model integration is discussed first, followed by a description of the differences from the standard model state resulting from changes to the assimilation system. Since the sea salt profiles are prescribed in the current version of the model and are not

affected by changes to the assimilation, sea salt aerosols are not included in the discussion of the sensitivity experiments. A complete characterization of the aerosol distribution and transport for the whole INDOEX intensive field program is given by *Rasch et al.* [this issue].

5.1. Aerosol Simulation in Standard Configuration

The mean aerosol optical depth for March 1–14, 1999, is shown in Plate 1. The model configuration used to calculate this optical depth will be described as the "standard" configuration hereafter. The model follows the description given in section 2, and the assimilation parameters are set to the values given in Table 2. The aerosol distributions for this 2-week period are representative of the distributions observed throughout the experiment. The AOD is generally <0.15 south of the equator. Areas with AOD exceeding 0.4 are located on the western coast of India close to Bombay, on the eastern coast of India close to Calcutta, and on the eastern side of the Bay of Bengal close to Myanmar. A plume of elevated AODs extends from the region around Bombay south and west over the Arabian Sea. Areas with AODs exceeding 0.3 are apparent over the Saudi Arabian peninsula and eastern Africa. The average optical depth retrieved from NOAA 14 data used in the assimilation is shown in Plate 2. The model and retrieved optical depths agree to within ±0.05 over most of the Indian Ocean, Bay of Bengal, and Arabian Sea. Somewhat larger differences occur in coastal regions west of India and immediately adjacent to major continental sources.

The mean aerosol optical depths for sulfate, dust, carbon, and sea salt are shown in Plate 3. It is evident that carbonaceous aerosols contribute most of the elevated AOD in the areas around Bombay, Calcutta, and Myanmar. There is a secondary maximum in the carbonaceous AOD over eastern Africa. The dominant contribution to the total AOD in the northwestern Arabian Sea and adjoining continental regions is from the mineral dust aerosols. The sulfate AOD is elevated in a plume-like structure extending from the western coast of India out over the Arabian Sea. The sea salt aerosols represent the largest component of the total AOD in the southern and eastern Indian Ocean. The local maximum in sea salt AOD at 90°E, 10°S is associated with a tropical cyclone with elevated surface wind speeds at that location.

Vertical profiles of the mass mixing ratios for sulfate, mineral dust, and carbonaceous aerosols are plotted in Plate 4. The mixing ratios are zonal averages over 70°E–75°E. This range includes the longitude for the INDOEX operations and observational facility on Hululé Island (4°12′N, 73°32′E) and the Kaashidhoo climate observatory (KCO, at 4°58′N, 73°28′E). All three aerosol types are concentrated at pressures greater than 700 hPa north of the equator, and all three have a local minimum between the surface and 900 hPa between 5° and 10°N. The maximum mass mixing ratios for dust and carbon are near the surface northward of 20°N and close to Bombay. There is a secondary maximum in the carbonaceous mixing ratios at ~800 hPa between 10° and 20°N. These spatial patterns are consistent with the location of the dominant sources of carbonaceous aerosols, sulfate precursors, and mineral dust aerosols in continental regions bordering the Arabian Sea.

The corrections applied by the assimilation tend to increase the AOD in coastal areas of the Indian subcontinent and to decrease the AOD in the northern Arabian Sea. The average multiplicative correction applied to the model fields by each assimilation step is shown in Plate 5. The correction factor is >1 over most of the Indian Ocean with the exception of areas north of Madagascar. The largest correction factors are collocated with coastal cities in India, including Karachi, Bombay, and Calcutta, and with coastal areas of southeast Asia and Indonesia. Although the satellite retrievals are only available over ocean areas, the corrections applied by the correction extend over adjacent continental regions. The extension to land surfaces is caused by the assumptions regarding horizontal covariance of errors and is discussed further in section 5.4. From (2) and (4) it follows that the maxima in the Indian coastal areas could result from an underestimate of the aerosol mass, errors in specification of optical extinction, or errors in the retrieval of AOD from the satellite imagery. The latter two possibilities will be examined in greater detail using INDOEX in situ observations and improved satellite retrieval algorithms (section 6).

Table 4. Mean Aerosol Optical Depths From Sensitivity Studies for March 1–14, 1999

Model Run[a]	AOD (KCO)	Bias/RMS Error[b]	AOD (0°–15°N, 70°–80°E)
Standard	0.261	−0.02 ± 0.04	0.271
No assimilation	0.153	−0.12 ± 0.05	0.182
χ_C = 4 m^2/g	0.256	−0.02 ± 0.04	0.260
f_o = 0.1	0.270	−0.01 ± 0.05	0.280
f_m = 1	0.274	−0.003 ± 0.05	0.283
ℓ_{mz} = 0.5 km	0.258	−0.02 ± 0.05	0.269
ℓ_{mx} = 500 km	0.277	−0.01 ± 0.05	0.300

[a]See Table 2 for description of assimilation parameters varied in sensitivity tests.

[b]Bias and RMS error are computed from differences of daily mean AOD relative to estimates of AOD at 675 nm from KCO Sun photometer data [*Satheesh and Ramanathan*, 2000].

The total AOD produced by the model compares well with preliminary estimates of AOD from Microtops Sun photometers [*Satheesh and Ramanathan*, 2000] operated at KCO during the INDOEX field phase (Plate 6a). The model AOD is calculated at 630 nm, and the Microtops AOD values are derived from observations of extinction of the direct solar beam at 675 nm. For an Ångström exponent of 1 the difference in wavelength introduces a 7% reduction in the modeled AODs to match the wavelength of the Microtops data. The time series starts on February 8, 1999, at the initiation of the model spin-up and ends on March 16, 1999. During the first 10 days of the simulation the model tends to underestimate the AOD. Between February 8 and March 16, the error in the daily mean AOD from the model relative to the Microtops data is −0.03 ± 0.06. During the March 1–14 time frame of the sensitivity studies the error in the daily mean AOD is −0.02 ± 0.04. The modeled AOD at KCO and over a region of the Indian Ocean southwest of the southern tip of India are summarized for the standard integration and each sensitivity study in Table 4. The corresponding time series of AOD from each study is plotted against the Microtops data in Plate 6b. A measure of the forecast skill has been computed by comparing the 24-hour AOD forecasts against the NOAA Pathfinder AOD retrievals at the validation time of each forecast. The mean and RMS errors in the forecasts for the region around the INDOEX operations center at Malé are similar to errors in the aerosol analysis relative to the surface instruments. The mean forecast

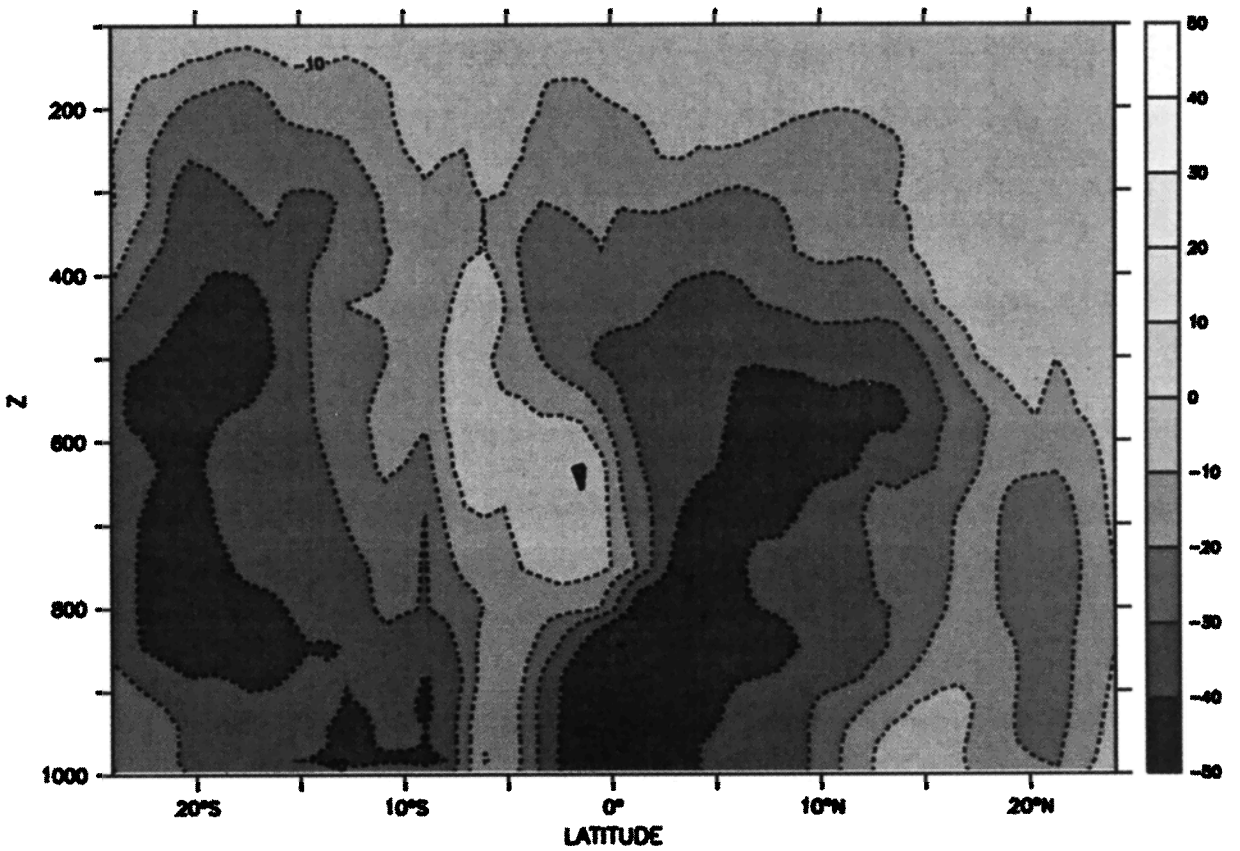

Figure 3. Percentage differences between aerosol mass-mixing ratios for sulfate from the simulation without assimilation and the standard integration. Changes for mineral dust and carbonaceous aerosols are very similar and are not plotted. Time period, spatial domain, and wavelength are identical to Plate 4.

error in AOD is in range of 0 to −0.05, and the RMS error is in the range of 0.05 to 0.1.

5.2. Differences Between Simulations With and Without Assimilation

The effects of assimilation on the aerosol fields has been determined by running the standard case without assimilation of satellite retrievals of AOD. Except for the omission of assimilation, the simulation without assimilation is identical to the standard configuration (section 5.1). The differences between the total AOD with and without assimilation are shown in Plate 7. With the exception of a few small areas in the Arabian Sea, omission of assimilation has reduced the AOD over most of the Indian Ocean. The largest reductions are located southwest of the southern tip of India and in the areas around Bombay, Calcutta, and Myanmar. These locations are also sites of large reductions in the carbonaceous and mineral dust AOD values (Plate 8). While the sulfate AOD is a minor component of the total AOD in this simulation of the Indian Ocean region, the sulfate AOD is also reduced by >50% in the region southwest of India and Sri Lanka. The relative changes in the vertical profiles of aerosol mass mixing ratios are shown in Figure 3. The mass mixing ratios for sulfate, dust, and carbon are reduced over most of the troposphere. The largest relative reductions in the Northern Hemisphere in all three species are located between ~0°–10°N and between the surface and 600 hPa.

For this region and time period, omission of assimilation significantly decreases the non sea salt aerosols in regions downwind of the primary continental sources, including the region around the KCO site. Given the close agreement between the base model and the surface observations at KCO shown in Plate 6a, the reduction in AOD without assimilation degrades the fidelity of the model simulation compared to surface observations.

5.3. Variation With Modifications to Aerosol Optical Properties

In a CTM simulation without assimilation of satellite retrievals, uncertainties in the aerosol optical properties would affect the estimation of AOD from the model but would not affect the simulated aerosol mixing ratios. Once assimilation of satellite retrievals is included in the modeling system, the specification of aerosol optical properties influences the action of the assimilation on the aerosol fields during the model integration (Figure 1). In this sensitivity study the effects of the changing the aerosol extinction on the simulation are studied by reducing the specific extinction of the carbonaceous aerosols from 9 to 4 m^2/g at 630 nm. The specific extinction of a carbonaceous aerosol can vary over a large range depending on its chemical and physical properties (section 2.5). It is subject to some of the largest uncertainties of any aerosol species in the absence of in situ observations. A value of 4 m^2/g at 630 nm is a plausible extinction for smoke aerosols [*Liousse et al.*, 1997].

The total AOD is reduced relative to the standard run by

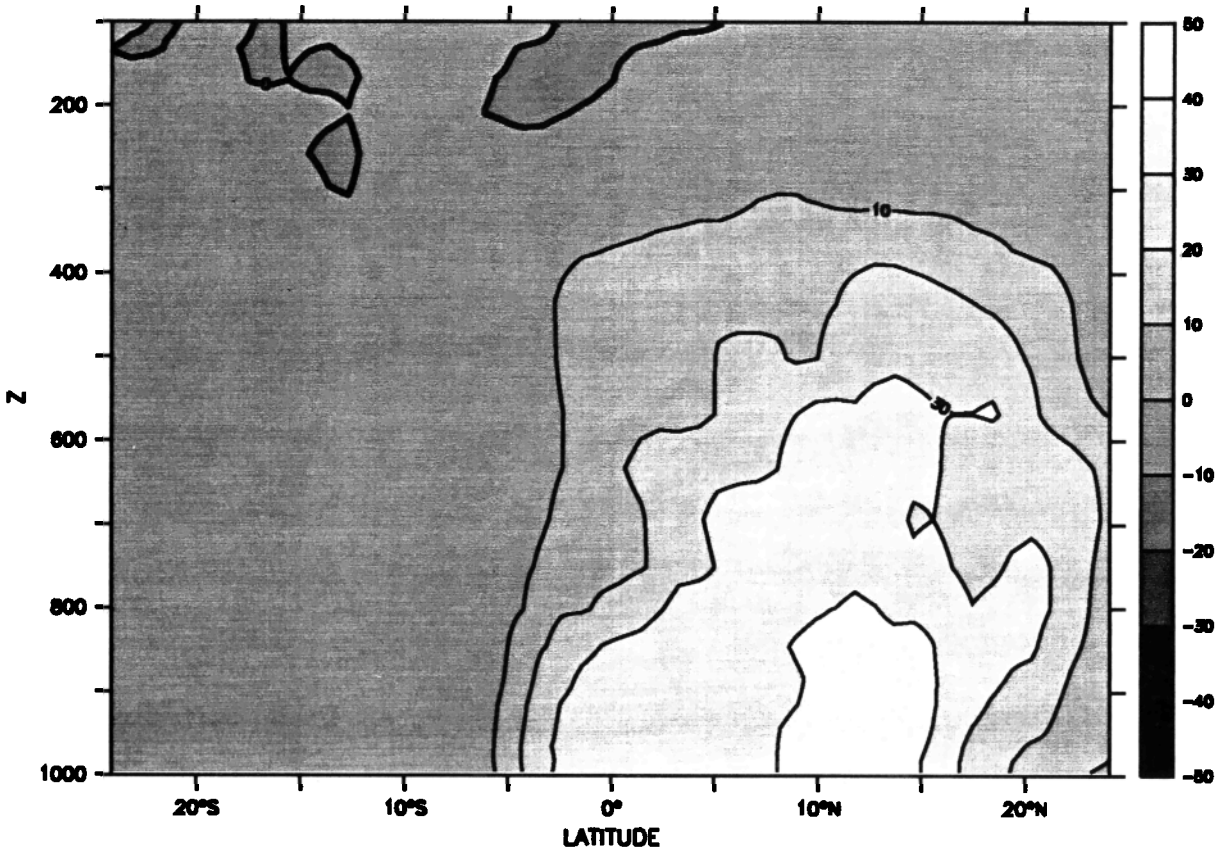

Figure 4. Percentage differences between aerosol mass-mixing ratios for sulfate from the simulation with $\chi_C = 4$ m^2/g and the standard integration with $\chi_C = 9$ m^2/g. Changes for mineral dust and carbonaceous aerosols are very similar and are not plotted. Time period, spatial domain, and wavelength are identical to Plate 4.

between 0.01 and 0.03 over most of the Arabian Sea and Bay of Bengal (Plate 9). The reductions over the Indian subcontinent, Bangladesh, and Myanmar are as large as 0.13. As expected, these reductions are caused by a decrease in the AOD of carbonaceous aerosols (Plate 10). The AOD of the carbonaceous aerosols is reduced over India, the Bay of Bengal, and the eastern half of the Arabian Sea (Plate 10). In the absence of assimilation, the AOD from carbon should be reduced by 4/9 of its original value in the standard run. It is evident from comparison of Plate 10 and Plate 3 that the change in the carbonaceous AOD is less than expected. It is also evident that the AOD contributed by sulfate and dust have simultaneously increased. The increase in dust AOD is comparable in magnitude to the decrease in carbonaceous AOD over the northern half of the Indian Ocean.

As noted in section 2.4, the relative corrections from the assimilation are applied uniformly to the sulfate, mineral dust, and carbonaceous aerosol fields in the current system. Lowering the specific extinction of carbon causes the assimilation system to increase the mass mixing ratios of all three aerosols in order to meet the boundary constraint imposed by the satellite AOD retrievals (Plate 11). The relative changes in the vertical profiles of the aerosol species are shown in Figure 4. The spatial distribution and magnitude of the percentage increases are very similar for the three species. The percentage increase in the carbon in the northern lower troposphere is nearly large enough to offset the percentage reduction in specific extinction. This example demonstrates that assimilation introduces a negative feedback between aerosol extinction and aerosol mass in the simulation system. The feedback follows from differentiating both sides of (2) assuming that $d\tau_m \simeq 0$ is imposed by the assimilation. These results suggest that there may be feedbacks related to other aerosol optical properties that affect satellite retrievals of AOD, for example, the aerosol phase functions and single-scattering albedos [*King et al.*, 1999]. Examination of these feedbacks will be undertaken in a separate study.

5.4. Variation With Free Parameters in Assimilation

There are seven free parameters in the assimilation package related to the magnitude and spatial correlation of errors in the models and observations (Table 2). These parameters govern the action of the assimilation on the model fields (section 2.4). For example, smaller values for the relative error f_o in the satellite retrievals or larger values for the relative error f_m in the model will generally yield larger corrections to the model fields. The values assigned to these parameters are preliminary and subject to change. Given the relatively large uncertainties, strong sensitivity to these parameters would be an undesirable feature of the aerosol assimilation system. The response of the simulated aerosol distributions has been examined for changes in the fractional error in the data (f_o), fractional error in the model (f_m), and the horizontal and vertical error-correlation length scales for the model (ℓ_{mx} and ℓ_{mz}, respectively).

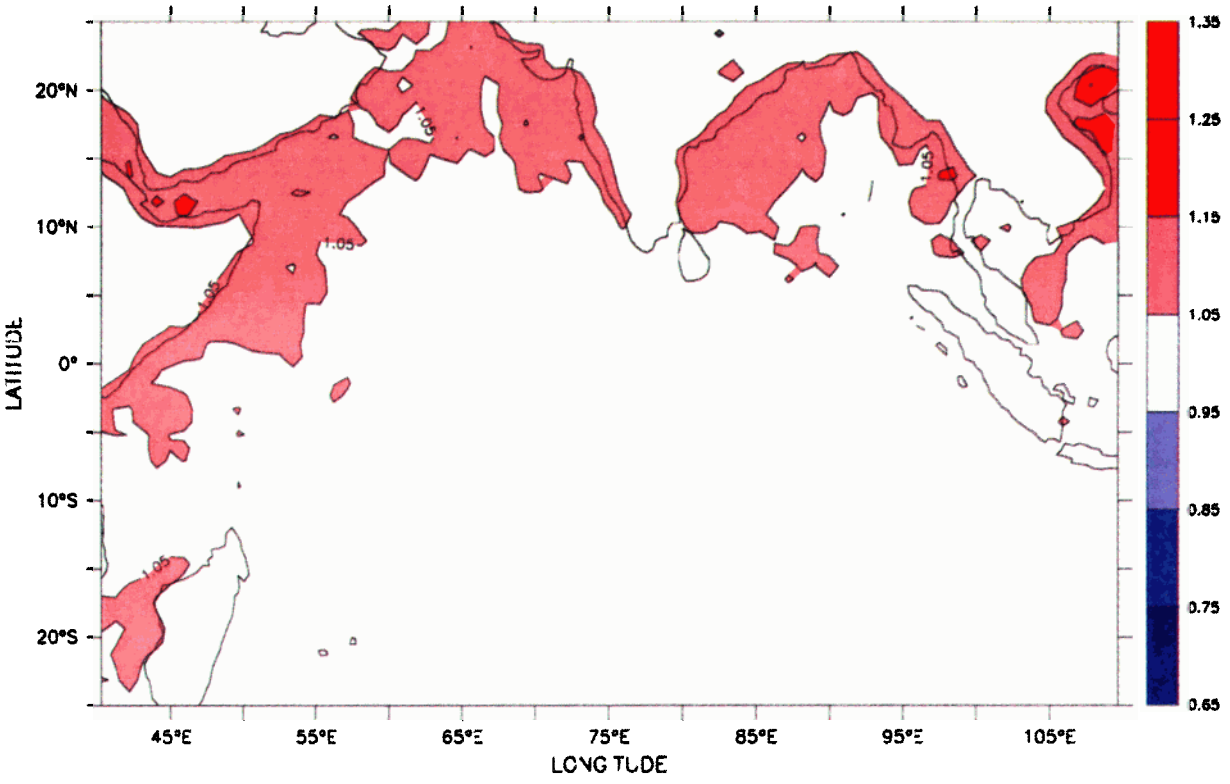

Plate 11. Ratio of multiplicative correction to the aerosol optical depth when $\chi_C = 4$ m^2/g to the average correction for the standard integration with $\chi_C = 9$ m^2/g.

The effects of reducing f_o by 50% to 0.1 are shown in Plate 12a. Because the absolute differences in AOD are quite small, the effects of reducing f_o have been plotted as relative differences in AOD. The most significant changes occur over coastal and land surfaces in areas adjacent to major anthropogenic sources for aerosols (section 5.1). This result may seem counterintuitive since the assimilation of satellite retrievals is operating only over ocean surfaces (section 3.2). However, the nonzero value of ℓ_{mx} implies that corrections applied in coastal regions by the assimilation extend over adjacent land surfaces as well. In addition, the differences between the model and observations should be larger in coastal regions than in more remote ocean regions. This tendency results from the presence of significant continental sources for aerosols and from the absence of satellite retrievals over land. Therefore reduction in the relative uncertainty in the satellite retrievals results in larger corrections to the model that are propagated over the surrounding continental regions. Note, however, that the relative changes in AOD are quite small (<15%) over the Indian subcontinent and southeast Asia (Plate 12a). The changes in aerosol mass mixing ratios are <10% for all species over most of the INDOEX region. The relative error f_o in the satellite retrieved AOD can in principle include systematic errors associated with an unrealistic aerosol optical model. It is certainly arguable that it would be more appropriate to increase f_o rather than decrease it. The maximum errors in a single-channel retrieval [e.g., *Stowe et al.*, 1997] can be as large as 100% [*Mishchenko and Travis*, 1997], and an analysis using a retrieval specially created for the aerosol found in the INDOEX region shows that the relative error may be as large as 30% [*Rajeev et al.*, 2000]. The qualitative effects of increasing f_o are to relax the solution back to the solution without assimilation discussed in section 5.2.

The effects of increasing f_m by 100% to 1 are shown in Plate 12b. As suggested above, the effects of increasing f_m should be qualitatively similar to the effects of reducing f_o. The resulting change in AOD supports this inference. In the Northern Hemisphere the AOD increases by up to 15% primarily over India, southeast Asia, and adjacent coastal areas. The increase in AOD extends over a larger area of the Arabian Sea southwest of India than in the integration with $f_o = 0.1$. The major difference between the runs with lower f_o and higher f_m is the increase in AOD in the south-eastern Indian Ocean. In the simulation with $f_m = 1$, the aerosol mass-mixing ratios increase by 10–30% in the lower and middle troposphere at latitudes beyond 10°S (Figure 5a). However since the mass-mixing ratios at those latitudes are <20% of the peak values in the Northern Hemisphere (Plate 4), the resulting changes in AOD are <0.03.

The reduction of ℓ_{mz} by 50% to 0.5 km changes the AODs by <0.01 over the entire Indian Ocean (not shown). The principle changes relative to the standard simulation are in the vertical distribution of aerosol mass-mixing ratios (Figure 5b). The mixing ratios increase between the surface and 800 hPa from 10°S to 20°N. The mixing ratios decrease over the rest of the troposphere. As shown in the comparison of the simulations with and without assimilation (section 5.2), assimilation increases the mass mixing ratios and AOD over the March 1–14 time period. In the limit where ℓ_{mz} is large compared to the model grid thickness, the corrections applied by the assimilation will be uniform in the vertical. As ℓ_{mz} is reduced to scales smaller than the depth of an individual model layer, the

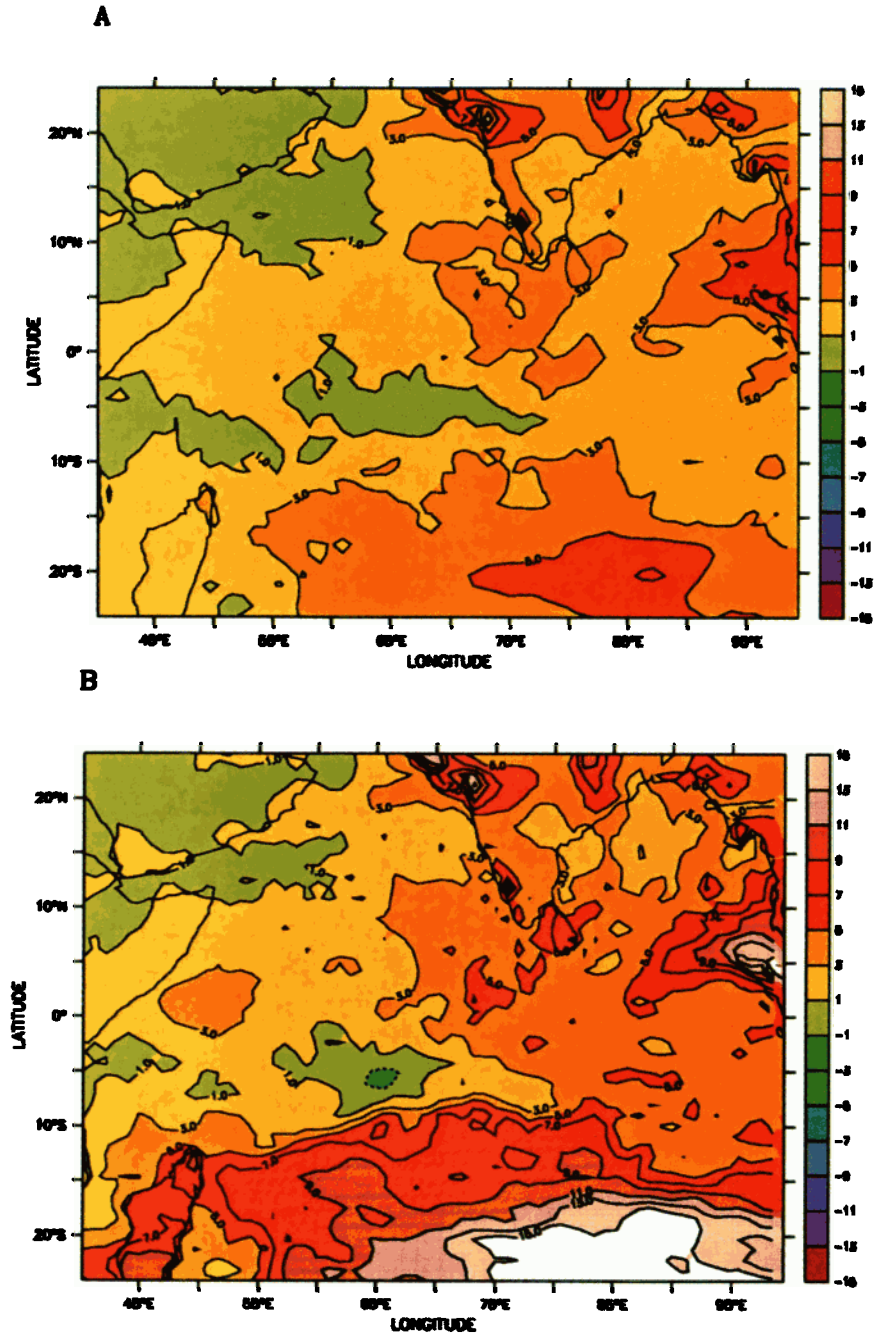

Plate 12. (a) Percentage differences between average aerosol optical depths from the simulation with the fractional observational error $f_o = 0.1$ and the standard integration with $f_o = 0.2$. (b) Percentage differences between average aerosol optical depths from the simulation with the fractional model error $f_m = 1$ and the standard integration with $f_m = 0.5$. Time period and wavelength are identical to Plate 1.

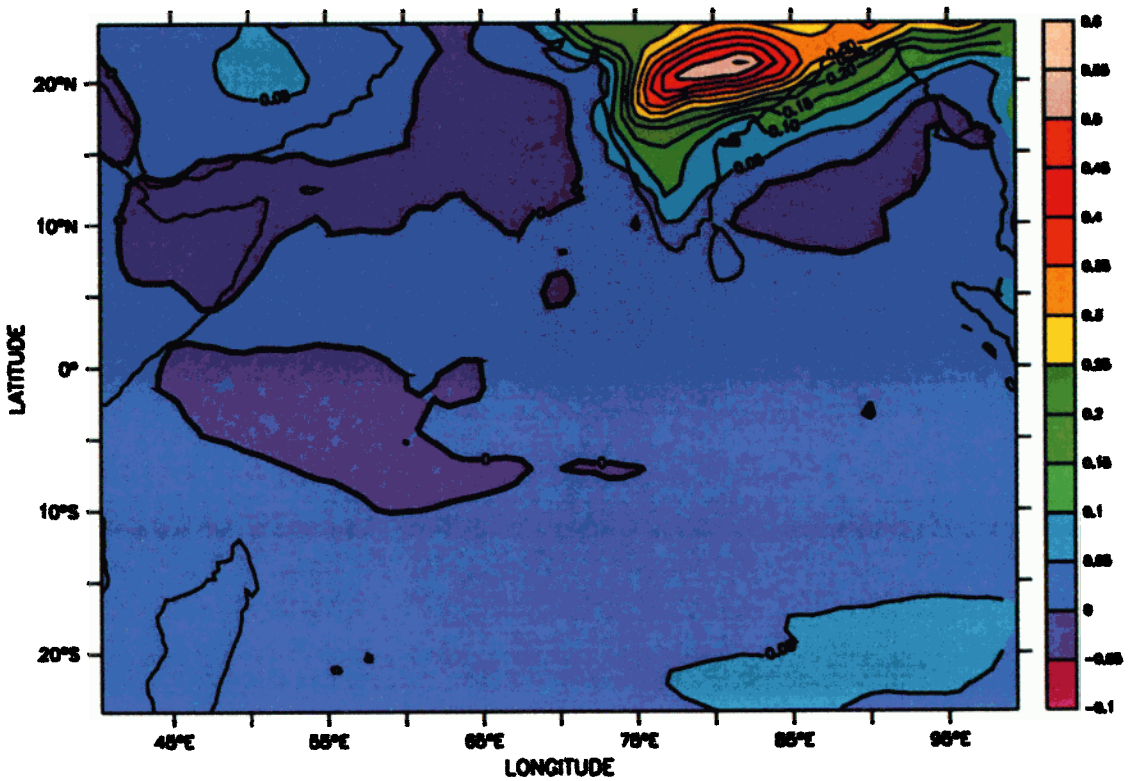

Plate 13. Differences between average aerosol optical depths from the simulation with the horizontal error correlation scale ℓ_{mz} = 500 km and the standard integration with ℓ_{mz} = 100 km. Time period and wavelength are identical to Plate 1.

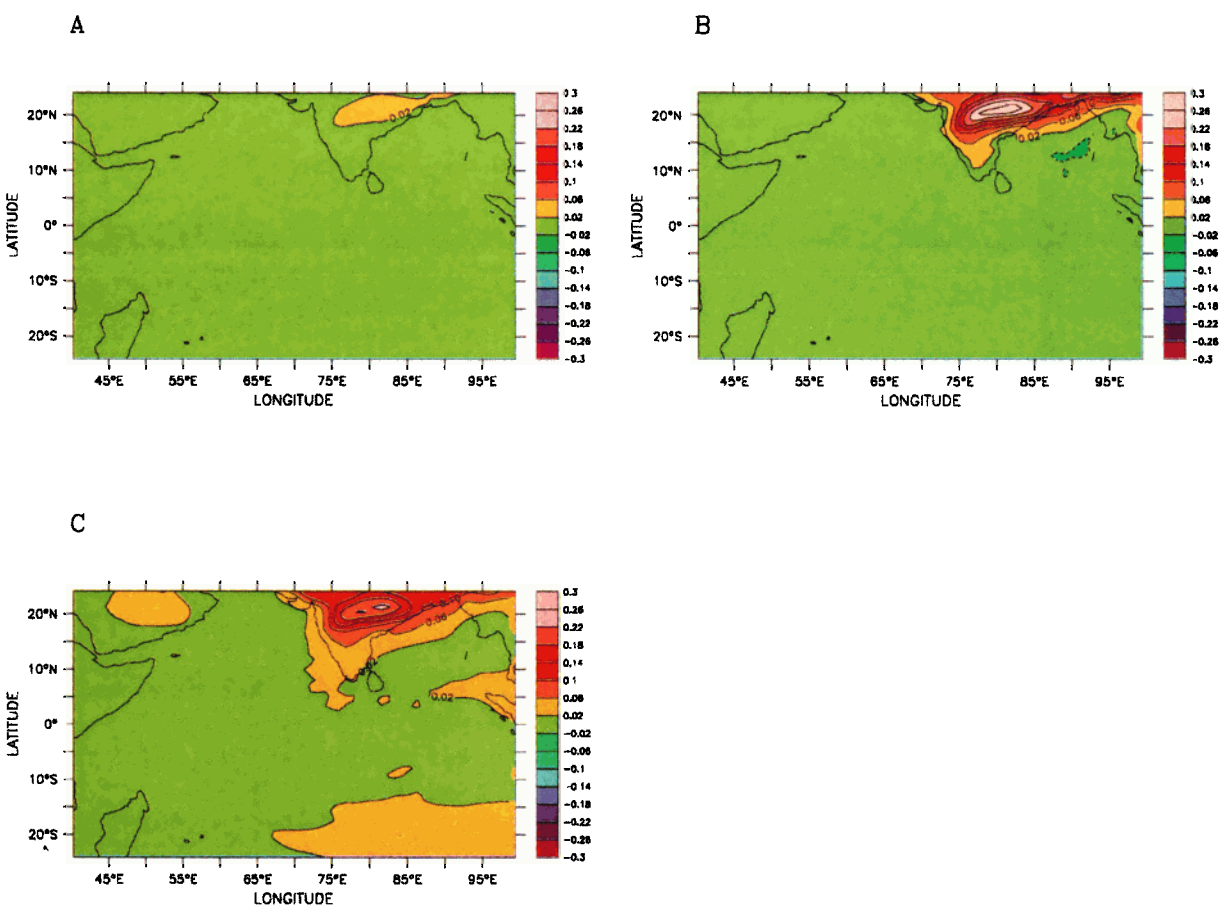

Plate 14. Differences between average aerosol optical depths for each aerosol species from the simulation with the horizontal error correlation scale ℓ_{mz} = 500 km and the standard integration with ℓ_{mz} = 100 km. Time period and wavelength are identical to Plate 3: (a) sulfate, (b) black and organic carbon, and (c) mineral dust.

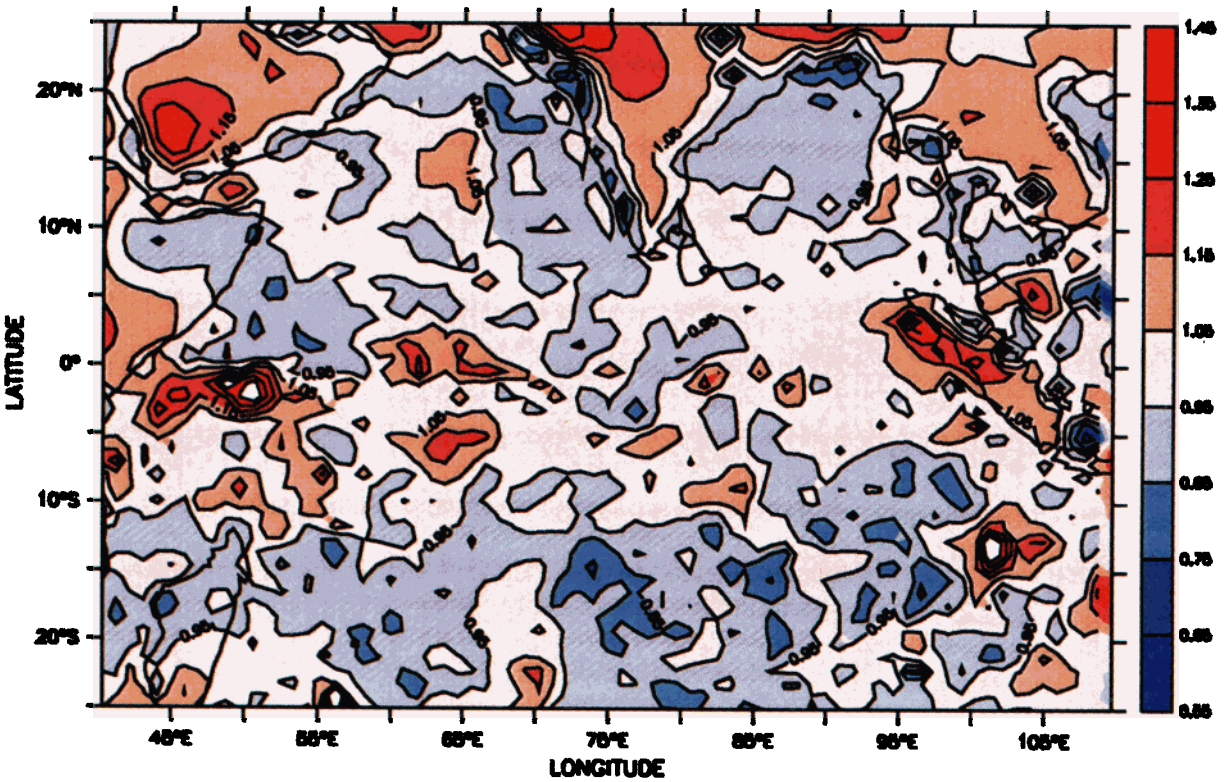

Plate 15. Ratio of multiplicative correction to the aerosol optical depth when the horizontal error correlation scale ℓ_{mx} = 500 km to the average correction for the standard integration with ℓ_{mx} = 100 km.

corrections applied by the assimilation should be increasingly correlated with the vertical mass distribution. In the standard simulation, most of the aerosol mass is concentrated in the lowest 300 hPa of the troposphere (Plate 4). Thus the effect of decreasing ℓ_{mz} is to reduce the aerosol mass at pressures less than 700 hPa and increase the aerosol mass near the surface.

The effects of changing the horizontal error-covariance length ℓ_{mx} from 100 to 500 km are larger AODs over continental source regions, particularly the Indian subcontinent, and larger AODs over the south-eastern Indian ocean (Plate 13). The AOD increases by up to 0.5 over central India. The increases are primarily associated with increased mineral-dust and carbonaceous aerosols (Plate 14). These changes result from the combination of large corrections applied by the assimilation in coastal regions together with a long horizontal length-scale for the application of these corrections (Plate 15). Analysis of data from LITE (section 2.4) suggests that 500 km is probably an overestimate of the horizontal correlation length scale for aerosols.

These results demonstrate that the simulated aerosol fields are relatively insensitive to changes in most of the free parameters in the assimilation. The changes in AOD introduced by variation of the parameters are much smaller than the changes associated with omission of assimilation or variation in aerosol optical properties (Table 4 and Figure 3b). This is an encouraging finding since the uncertainties in those parameters are not known but could be large. It should be noted that this conclusion is based on examination of a limited sample of model output and may not apply to other configurations of aerosol assimilation.

6. Future Developments

During the INDOEX field phase the aerosol observations available for assimilation were limited to satellite retrievals. However, the assimilation package can be readily extended to ingest aerosol data from ships, surface sites, and aircraft. These data include multiwavelength aerosol optical depths from spectral radiometers, estimates of optical depths for each aerosol species from detailed microphysical and chemical measurements, and vertical lidar profiles of aerosol backscatter [*Ramanathan et al.*, 1996]. The lidar data will be particularly useful in improving the representation of the vertical stratification of aerosols in the model. While the assimilation of column-integrated quantities does modify the vertical aerosol distribution through the assumption of vertical autocorrelation of errors (equation (7)) and the definition of **H**, the assimilation will only guarantee that the measured and modeled column-integrated quantities are consistent. The vertical redistribution of aerosol using lidar data should affect the subsequent transport of the aerosol constituents. The assimilation of aerosol optical depth for each species and aerosol size category will remove the indeterminacy of the current assimilation process (section 2.4). We also plan to replace the satellite retrievals of optical depths with retrievals based upon aerosol models constructed using INDOEX observations from the IFP and earlier INDOEX field observations [*Rajeev et al.*, 2000].

In addition, the in situ observations can be used to determine or constrain parameters in the assimilation system. The INDOEX observations include estimates of extinction for each species of aerosol currently included in the model. These data

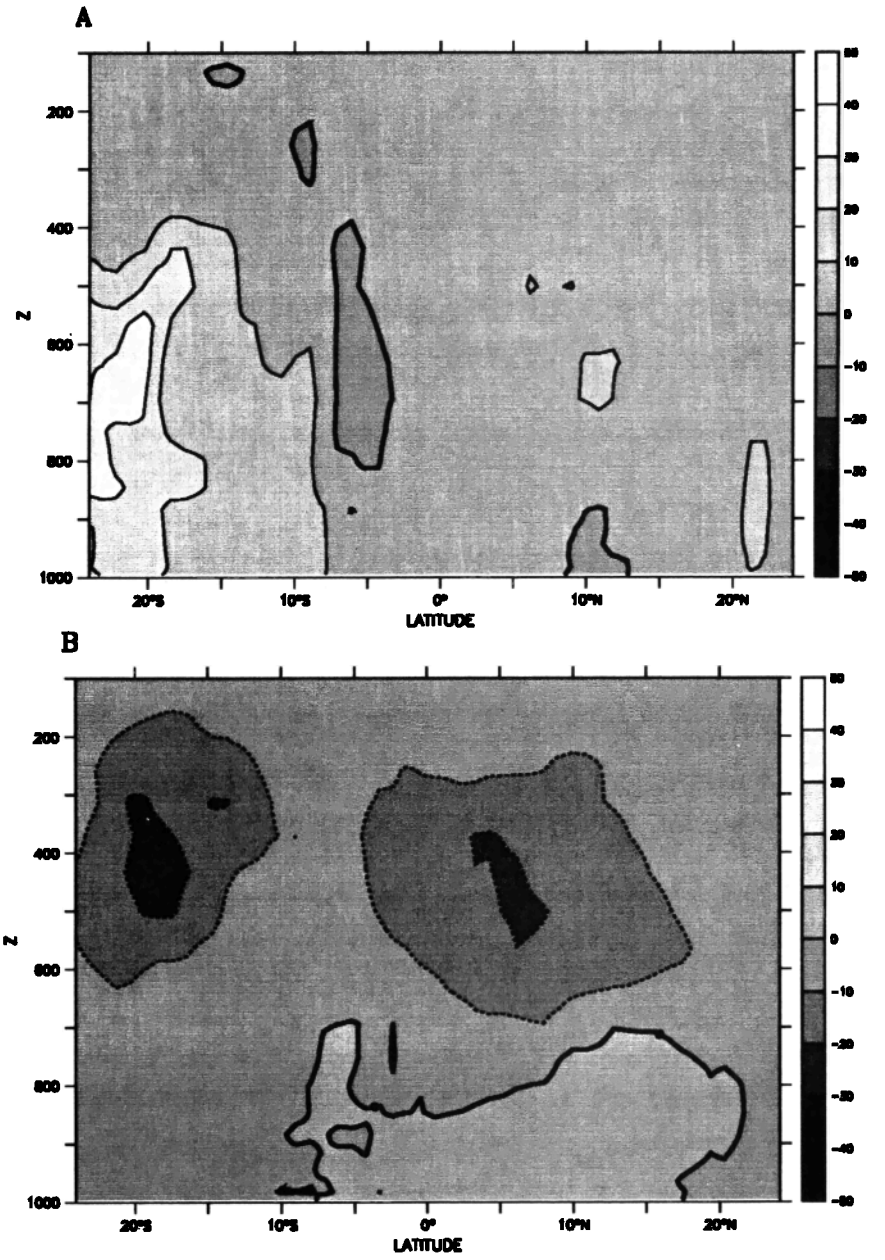

Figure 5. (a) Percentage differences between aerosol mass-mixing ratios for sulfate from the simulation with the fractional model error $f_m = 1$ and the standard integration with $f_m = 0.5$. Changes for mineral dust and carbonaceous aerosols are very similar and are not plotted. (b) Percentage differences between aerosol mass-mixing ratios for sulfate from the simulation with the vertical error correlation scale $\ell_{mz} = 0.5$ km and the standard integration with $\ell_{mz} = 1.0$ km. Changes for mineral dust and carbonaceous aerosols are very similar and are not plotted. Time period, spatial domain, and wavelength are identical to Plate 4.

will help reduce the large uncertainties in, for example, the extinction of the carbonaceous species (section 5.3). The new estimates of optical extinction will affect both the action of the assimilation on the model (section 2.4) and the forecasts of aerosol optical depth produced by the model from (2). The hygroscopic growth of the various aerosols has also been measured. The theoretical hygroscopic growth factors in the assimilation (equation (8)) will be replaced with the measured functions evaluated using in situ values of the relative humidity. The improvements in the assimilation system and assimilated data will be used to generate a four-dimensional gridded aerosol analysis for INDOEX.

Future versions of the assimilation system will incorporate several improvements to the parameterization of aerosols. The sulfate module will include an explicit representation of mass and number for coarse and accumulation-mode aerosols in an enhancement to the formulation of *Kreidenweis et al.* [1995]. This will provide a substantial improvement in the representation of aerosol optics, the interaction of sulfate aerosols with cloud microphysics, and the characterization of new particle

formation. The very crude diagnostic prescription for sea-salt will soon be replaced with a prognostic formulation similar to *Gong et al.* [1997a, 1997b]. A detailed microphysical scheme for dust mobilization is being developed and tested in MATCH and the NCAR CCM. Finally, the CSM land surface model (LSM) may be included as a new component in MATCH. Incorporation of LSM can improve the physical descriptions of land properties relevant to dust mobilization, dry deposition, and emission of volatile organic carbon compounds.

Using data from several upcoming satellite sensors, it should be possible to extend the aerosol analysis to most of the globe. These sensors include the Moderate Resolution Imaging Spectrometer (MODIS) and Multi-angle Imaging Spectrometer (MISR) on the NASA Terra satellite and several new instruments on European and Japanese platforms [*King et al.*, 1999]. MODIS is an internally calibrated imager with channels at 36 discrete spectral bands. MISR is a multi-angle imager with channels at 4 discrete spectral bands. Aerosol optical depths over land and ocean will be retrieved from MODIS imagery [*King et al.*, 1992; *Kaufman et al.*, 1997; *Tanré et al.*, 1997] and MISR observations [*Martonchik and Diner*, 1992; *Kahn et al.*, 1998]. The assimilation of these new satellite data sets should improve the fidelity of the solution and reduce the sensitivity of the model over land surfaces to poorly known parameters in the assimilation scheme. The vertical distribution of aerosols will be determined from space-borne lidars on the satellites Ice, Cloud, and land Elevation Satellite (ICESat) and the Pathfinder Instruments For Cloud And Aerosol Spaceborne Observations-Climatologie Etendue des Nuages et des Aerosols (PICASSO-CENA). Data from the Geoscience Laser Altimeter System (GLAS) on ICESat will be used to retrieve vertical profiles of aerosol extinction. The PICASSO-CENA mission will be launched into a nearly identical orbit with the EOS-PM satellite. The coincident data from the two platforms will provide observations of aerosol properties, spatial distribution, and direct radiative forcing using passive and active remote sensing.

7. Conclusions

A system for modeling the distribution and evolution of aerosols has been developed by combining a chemical transport model and an assimilation package for aerosol observations. The model simulates sea-salt, sulfate, carbonaceous, and dust aerosols together with tracers used to diagnose transport of the aerosol constituents. To assimilate aerosol optical properties, the model fields are converted to estimates of these properties using an aerosol optics package. In its first application the system has been used to forecast aerosol optical depth for planning the deployment of ships and aircraft during the Indian Ocean Experiment. Comparison of the analysis based on satellite retrievals against Sun photometer data shows that the system can accurately track daily variations in the aerosol optical depth at a single grid point.

The assimilation system can form the basis for new techniques for evaluating and improving the treatment of aerosols in CTMs. The enhancements include better representations of sources and removal processes. CTMs coupled with variational assimilation have already been developed to characterize source emissions of trace gases [*Robertson and Langner*, 1998]. The incorporation of assimilation is an extension of classical inverse methods for deducing source strengths with CTMs alone [*Hartley and Prinn*, 1993; *Mahowald et al.*, 1997]. The application of inverse methods could help reduce the large uncertainties in the emissions of aerosol precursors.

The system will be used to construct a gridded aerosol estimate for INDOEX by assimilating satellite retrievals of aerosol optical depth and data from surface and airborne instrumentation. This will allow the extension of the in situ observations to the scale of the Indian Ocean. The combination of satellite data and aerosol assimilation could also be used to produce a global gridded aerosol analysis consistent with the constraints imposed by the observations. The resulting global data set could be used to compute the direct radiative forcing by aerosols with unprecedented accuracy.

Acknowledgments. The authors are grateful to L. Stowe and A. Ignatov (NOAA) for providing the code to the NOAA Pathfinder aerosol retrieval algorithm. The assistance of M. Bradford and N. Gamage (UCAR) in acquiring real-time NOAA AVHRR LAC data and S. Williams (UCAR) and T. Cremidis (NOAA) in acquiring NOAA AVHRR GAC data is gratefully acknowledged. The authors wish to thank S. Dobbie (Dalhousie Univ.) and P. Quinn (NOAA PMEL) for parameterizations and information regarding optical properties of sea-salt aerosols. J. Penner (U. Michigan) generously provided data sets for sources of carbonaceous aerosols. H.-L. Pan (NCEP) assisted in the acquisition and interpretation of NCEP aviation analyses and forecasts in near real-time. M. Lawrence (MPI) helped develop the time-line for the operational forecasts during INDOEX and shared the results of his MATCH simulations of tropospheric chemical constituents. The authors wish to thank J. Prospero (U. Miami) and A. Clark (U. Hawaii) for numerous discussions regarding their in situ observations of aerosol chemical composition. V. Ramanathan and S. K. Satheesh (SIO/UCSD) kindly provided their Microtops sunphotometer data for evaluation of the aerosol optical depths computed from the assimilation system. P. Durkee and K. Nielsen (Naval Postgraduate School) processed the AVHRR data from INDOEX using their aerosol retrieval method and shared the resulting data set with the authors. Discussions with J. Kiehl (NCAR) were instrumental in the evaluation of the assimilation system. This research has been supported by NASA Grant MTPE S-97889-F (WDC), NSF award ATM9405024 to the Center for Clouds, Chemistry, and Climate (PJR and BEE), and NSF INDOEX grant ATM9612887 (PJR). BVK was supported by the NASA UARS project under NRA-97-MTPE-04 (contract S10109-X), the NASA MOPITT project, and the National Center for Atmospheric Research. JFL and CSZ were supported by the NASA Earth Observing System (EOS) Grant 87391-F. The National Center for Atmospheric Research is sponsored by the National Science Foundation.

References

Austin, J., Toward the four-dimensional assimilation of stratospheric chemical constituents, *J. Geophys. Res.*, *97*, 2569–2588, 1992.

Barth, M. C., P. J. Rasch, J. T. Kiehl, C. M. Benkovitz, and S. E. Schwartz, Sulfur chemistry in the National Center for Atmospheric Research Community Climate Model: Description, evaluation, features and sensitivity to aqueous chemistry, *J. Geophys. Res.*, *105*, 1387–1415, 2000.

Benkovitz, C. M., M. T. Scholz, J. Pacyna, L. Tarrason, J. Dignon, E. C. Voldner, P. A. Spiro, J. A. Logan, and T. E. Graedel, Global gridded inventories of anthropogenic emissions of sulfur and nitrogen, *J. Geophys. Res.*, *101*, 29,239–29,253, 1996.

Blanchard, D. C., and A. H. Woodcock, Production, concentration, and vertical distribution of the sea salt aerosol, *Ann. New York Acad. Sci.*, *338*, 330–347, 1980.

Bonan, G. B., A land surface model (LSM version 1.0) for ecological, hydrological, and atmospheric studies: Technical description and user's guide, *Tech. Rep. NCAR/TN-417+STR*, 150 pp., Natl. Cent. for Atmos. Res., Boulder, Colo., Jan. 1996.

Caplan, P., J. Derber, W. Gemmill, and S. Y. Hong, Changes to the 1995 NCEP operational medium-range forecast model analysis-forecast system, *Weather Forecasting*, *12*, 581–594, 1997.

Charlson, R. J., S. E. Schwartz, J. M. Hales, R. D. Cess, J. J. A.

Coakley, J. E. Hansen, and D. J. Hofmann, Climate forcing by anthropogenic aerosols, *Science*, *255*, 423–430, 1992.

Cooke, W. F., and J. J. N. Wilson, A global black carbon aerosol model, *J. Geophys. Res.*, *101*, 19,395–19,409, 1996.

Cooke, W. F., C. Liousse, H. Cachier, and J. Feichter, Construction of a 1 degrees x 1 degrees fossil fuel emission data set for carbonaceous aerosol and implementation and radiative impact in the ECHAM4 model, *J. Geophys. Res.*, *104*, 22,137–22,162, 1999.

d'Almeida, G. A., P. Koepke, and E. P. Shettle, *Atmospheric Aerosols. Their Global Climatology and Radiative Characteristics*, 561 pp., A. Deepak, Hampton, Va., 1991.

Elbern, H., and H. Schmidt, A four-dimensional variational chemistry data assimilation scheme for Eulerian chemistry transport modeling, *J. Geophys. Res.*, *104*, 18,583–18,598, 1999.

Elbern, H., H. Schmidt, and A. Ebel, Variational data assimilation for tropospheric chemistry modeling, *J. Geophys. Res.*, *102*, 15,967–15,985, 1997.

Fisher, M., and D. J. Lary, Lagrangian four-dimensional variational data assimilation of chemical species, *Q. J. R. Meteorol. Soc.*, *121*, 1681–1704, 1995.

Gong, S. L., L. A. Barrie, and J.-P. Blanchet, Modeling sea-salt aerosols in the atmosphere, 1, Model development, *J. Geophys. Res.*, *102*, 3805–3818, 1997a.

Gong, S. L., L. A. Barrie, J. M. Prospero, D. L. Savoie, G. P. Ayers, J.-P. Blanchet, and L. Spacek, Modeling sea-salt aerosols in the atmosphere, 2, Atmospheric concentrations and fluxes, *J. Geophys. Res.*, *102*, 3819–3830, 1997b.

Guenther, A., et al., A global model of natural volatile organic compound emissions, *J. Geophys. Res.*, *100*, 8873–8892, 1995.

Hartley, D., and R. Prinn, Feasibility of determining surface emissions of trace gases using an inverse method in a three-dimensional chemical transport model, *J Geophys. Res*, *98*, 5183–5197, 1993.

Haywood, J. M., D. L. Roberts, A. Slingo, J. M. Edwards, and K. P. Shine, General circulation model calculations of the direct radiative forcing by anthropogenic sulfate and fossil-fuel soot aerosol, *J. Clim.*, *10*, 1562–1577, 1997.

Haywood, J. M., and V. Ramaswamy, Global sensitivity studies of the direct radiative forcing due to anthropogenic sulfate and black carbon aerosols, *J Geophys. Res.*, *103*, 6043–6058, 1998.

Herman, J. R., P. K. Bhartia, O. Torres, C. Hsu, C. Seftor, and E. Celarier, Global distributions of UV-absorbing aerosols from Nimbus 7/TOMS data, *J. Geophys. Res.*, *102*, 16,911–16,922, 1997.

Intergovernmental Panel on Climate Change, *Climate Change, 1995: The Science of Climate Change*, edited by J. T. Houghton et al., Cambridge Univ. Press, New York, 1996.

Jayaraman, A., D. Lubin, S. Ramachandran, V. Ramanathan, E. Woodbridge, W. D. Collins, and K. S. Zalpuri, Direct observations of aerosol radiative forcing over the tropical Indian Ocean during the Jan.-Feb. 1996 Pre-INDOEX cruise, *J. Geophys. Res.*, *103*, 13,827–13,836, 1998.

Kahn, R., P. Banerjee, D. McDonald, and D. J. Diner, Sensitivity of multiangle imaging to aerosol optical depth and to pure-particle size distribution and composition over ocean, *J. Geophys. Res.*, *103*, 32,195–32,213, 1998.

Kalnay, E., et al., The NCEP/NCAR 40-year reanalysis project, *Bull. Am. Meteorol. Soc.*, *77*, 437–471, 1996.

Kasibhatla, P., W. L. Chameides, and J. S. John, A three-dimensional global model investigation of seasonal variations in the atmospheric burden of anthropogenic sulfate aerosols, *J. Geophys. Res.*, *102*, 3737–3759, 1997.

Kaufman, Y. J., D. Tanré, L. A. Remer, E. F. Vermote, A. Chu, and B. N. Holben, Operational remote sensing of tropospheric aerosol over land from EOS moderate resolution imaging spectroradiometer, *J. Geophys. Res.*, *102*, 17,051–17,067, 1997.

Kettle, A. J., M. O. Andreae, D. Amouroux, and T. W. Andreae, A global database of sea surface dimethylsulfide (DMS) measurements and a procedure to predict sea surface DMS as a function of latitude, longitude, and month, *Global Biogeochem. Cycles*, *13*, 399–444, 1999.

Kidwell, K. B., *NOAA Polar Orbiter Data User's Guide*, NOAA, NESDIS, NCDC, Suitland, Md., 1998. (Available as http://www2.ncdc.noaa.gov/docs/podug)

Kiehl, J. T., J. J. Hack, G. B. Bonan, B. B. Boville, D. L. Williamson, and P. J. Rasch, The National Center for Atmospheric Research Community Climate Model: CCM3, *J Clim.*, *11*, 1131–1149, 1998.

Kiehl, J. T., T. L. Schneider, P. J. Rasch, M C. Barth, and J. Wong, Radiative forcing due to sulfate aerosols from simulations with the National Center for Atmospheric Research Community Climate Model, Version 3, *J. Geophys. Res.*, *105*, 1441–1457, 2000.

King, M. D., Y. J. Kaufman, W. P. Menzel, and D. Tanré, Remote sensing of cloud, aerosol, and water vapor properties from the Moderate Resolution Imaging Spectrometer (MODIS), *IEEE Trans. Geosci. Remote Sens.*, *30*, 2–27, 1992.

King, M. D., Y. J. Kaufman, D. Tanré, and T. Nakajima, Remote sensing of tropospheric aerosols from space: Past, present, and future, *Bull. Am. Meteorol. Soc.*, *80*, 2229–2259, 1999.

Kreidenweis, S. M., D. Y. Harrington, J. J. Walton, and J. E. Penner, Preliminary results from a two-moment aerosol model applied to a three-dimensional model of the global sulfur cycle, *Pap. 594*, 48 pp., Dep. of Atmos. Sci., Colo. State Univ., Fort Collins, 1995.

Krishnamurti, T. N., B. Jha, P. J. Rasch, and V. Ramanathan, A high resolution global reanalysis highlighting the winter monsoon, 1, Reanalysis fields, *Meteorol. Atmos. Phys.*, *64*, 123–150, 1997a.

Krishnamurti, T. N., B. Jha, P. J. Rasch, and V. Ramanathan, A high resolution global reanalysis highlighting the winter monsoon, 2, Transients and passive tracer transports, *Meteorol. Atmos. Phys.*, *64*, 151–171, 1997b.

Lamarque, J.-F., B. Khattatov, J. Gille, and G. Brasseur, Assimilation of Measurement of Air Pollution from Space (MAPS) CO in a global three-dimensional model, *J. Geophys. Res.*, *104*, 26,209–26,218, 1999.

Levelt, P. F., B. V. Khattatov, J. C. Gille, G. P. Brasseur, X. X. Tie, and J. Waters, Assimilation of the MLS ozone measurements in the global three-dimensional chemistry-transport model ROSE, *Geophys. Res. Lett.*, *25*, 4493–4496, 1998.

Liousse, C., J. E. Penner, C. Chuang, J. J. Walton, H. Eddleman, and H. Cachier, A global three-dimensional model study of carbonaceous aerosols, *J. Geophys. Res.*, *101*, 19,411–19,432, 1996.

Liousse, C., F. Dulac, H. Cachier, and D. Tanré, Remote sensing of carbonaceous aerosol production by African savanna biomass burning, *J. Geophys. Res.*, *102*, 5895–5911, 1997.

Lorenc, A. C., Analysis methods for numerical weather prediction, *Q. J. R. Meteorol. Soc.*, *112*, 1177–1194, 1986.

Mahowald, N. M., R. G. Prinn, and P. J Rasch, Deducing CCl_3F emissions using an inverse method and chemical transport models with assimilated winds, *J. Geophys. Res.*, *102*, 28,153–28,168, 1997.

Martonchik, J. V., and D. J. Diner, Retrieval of aerosol and land surface optical properties from multi-angle satellite imagery, *IEEE Trans. Geosci. Remote Sens.*, *30*, 223–230, 1992.

Mishchenko, M. I., and L. D. Travis, Satellite retrieval of aerosol properties over the ocean using polarization as well as intensity of reflected sunlight, *J. Geophys. Res.*, *102*, 16,989–17,013, 1997.

Parrish, D. F., J. C. Derber, R. J. Purser, and W. S. Wu, The NCEP global analysis system: Recent improvements and future plans, *J. Meteorol. Soc. Jpn.*, *75*, 359–365, 1997.

Patterson, E. M., Optical properties of the crustal aerosol: Relation to chemical and physical characteristics, *J. Geophys. Res.*, *86*, 3236–3246, 1981.

Patterson, E. M., and D. A. Gillette, Measurements of visibility vs. mass-concentration for airborne soil particles, *Atmos. Environ.*, *11*, 193–196, 1977.

Penner, J., Quantifying and minimizing uncertainty of climate forcing by anthropogenic aerosols, technical report, 53 pp., U.S. Dep. of Energy, Washington, D. C., 1993.

Penner, J. E., H. Eddleman, and T. Novakov, Towards the development of a global inventory for black carbon emissions, *Atmos. Environ.*, *27*, 1277–1295, 1993.

Quinn, P. K., and D. J. Coffman, Comment on "Contribution of different aerosol species to the global aerosol extinction optical thickness: Estimates from model results" by Tegen et al., *J. Geophys Res.*, *104*, 4241–4248, 1999.

Rajeev, K., V. Ramanathan, and J. Meywerk, Regional aerosol distribution and its long range transport over the Indian Ocean, *J. Geophys. Res.*, *105*, 2029–2043, 2000.

Ramanathan, V., et al., Indian Ocean Experiment (INDOEX), A multi-agency proposal for a field experiment in the Indian Ocean, technical report, Cent. for Clouds, Chem., and Climate (C4), Scripps Instit. of Oceanogr., Univ. of Calif., San Diego, June 1996.

Rasch, P. J., and J. E. Kristjánsson, A comparison of the CCM3 model climate using diagnosed and predicted condensate parameterizations, *J. Clim.*, *11*, 1587–1614, 1998.

Rasch, P J., N. M. Mahowald, and B. E. Eaton, Representations of

transport, convection, and the hydrologic cycle in chemical transport models: Implications for the modeling of short-lived and soluble species, *J. Geophys. Res.*, *102*, 28,127–28,138, 1997.

Rasch, P. J., et al., A comparison of scavenging and deposition processes in global models: Results from the WCRP Cambridge workshop of 1995, *Tellus*, *52*, 1025–1056, 2000a.

Rasch, P. J., M. C. Barth, J. T. Kiehl, S. E. Schwartz, and C. M. Benkovitz, A description of the global sulfur cycle and its controlling processes in the National Center for Atmospheric Research Community Climate Model, Version 3, *J. Geophys. Res.*, *105*, 1367–1385, 2000b.

Rasch, P. J., W. D. Collins, and B. E. Eaton, Understanding the Indian Ocean Experiment (INDOEX) aerosol distributions with an aerosol assimilation, *J. Geophys. Res.*, this issue.

Rhoads, K. P., P. Kelley, R. Dickerson, T. Carsey, M. Farmer, D. Savoie, and J. Prospero, The composition of the troposphere over the Indian Ocean during the monsoonal transition, *J. Geophys. Res.*, *102*, 18,981–18,995, 1997.

Robertson, L., and J. Langner, Source function estimate by means of variational data assimilation applied to the ETEX-I tracer experiment, *Atmos. Environ.*, *32*, 4219–4225, 1998.

Satheesh, S. K., and V. Ramanathan, Large differences in tropical aerosol forcing at the top of the atmosphere and Earth's surface, *Science*, *405*, 60–63, 2000.

Schulz, M., Y. J. Balkanski, W. Guelle, and F. Dulac, Role of aerosol size distribution and source location in a three-dimensional simulation of a Saharan dust episode tested against satellite-derived optical thickness, *J. Geophys. Res.*, *103*, 10,579–10,592, 1998.

Seinfeld, J. H., and S. N. Pandis, *Atmospheric Chemistry and Physics*, John Wiley, New York, 1997.

Shettle, E. P., Optical and radiative properties of a desert aerosol model, in *IRS '84: Current Problems in Atmospheric Radiation*, pp. 74–77, A. Deepak, Hampton, Va., 1984.

Shettle, E. P., and R. Fenn, Models of the atmospheric aerosols and their optical properties, paper presented at the Electromagnetic Wave Propagation Panel Symposium, Lyngby, Denmark, Oct. 27–31, 1975.

Stowe, L. L., A. M. Ignatov, and R. R. Singh, Development, validation, and potential enhancements to the second-generation operational aerosol product at the National Environmental Satellite, Data, and Information Service of the National Oceanic and Atmospheric Administration, *J. Geophys. Res.*, *102*, 16,889–16,910, 1997.

Stowe, L. L., P. A. Davis, and E. P. McClain, Scientific basis and initial evaluation of the CLAVR-1 global clear/cloud classification algorithm for the Advanced Very High Resolution Radiometer, *J. Atmos. Ocean. Tech.*, *16*, 656–681, 1998.

Tanré, D., Y. J. Kaufman, M. Herman, and S. Mattoo, Remote sensing of aerosol properties over oceans using the MODIS/EOS spectral radiances, *J. Geophys. Res.*, *102*, 16,971–16,988, 1997.

Tegen, I., and I. Fung, Modeling of mineral dust in the atmosphere: Sources, transport, and optical thickness, *J. Geophys. Res.*, *99*, 22,897–22,914, 1994.

Tegen, I., and A. A. Lacis, Modeling of particle size distribution and its influence on the radiative properties of mineral dust aerosol, *J. Geophys. Res.*, *101*, 19,237–19,244, 1996.

Tegen, I., P. Hollrig, M. Chin, I. Fung, D. Jacob, and J. Penner, Contribution of different aerosol species to the global aerosol extinction optical thickness: Estimates from model results, *J. Geophys. Res.*, *102*, 23,895–23,915, 1997.

Twomey, S. A., M. Piepgrass, and T. L. Wolfe, An assessment of the impact of pollution on global cloud albedo, *Tellus*, *36*, 356–366, 1984.

Wesely, M. L., and B. B. Hicks, A review of the current status of knowledge on dry deposition, *Atmos. Environ.*, *34*, 2261–2282, 2000.

Winker, D. M., R. H. Couch, and M. P. McCormick, An overview of LITE: NASA's Lidar In-space Technology Experiment, *Proc. IEEE*, *84*, 164–180, 1996.

W. D. Collins, B. E. Eaton, and P. J. Rasch, Climate and Global Dynamics Division, National Center for Atmospheric Research, P.O. Box 3000, Boulder, CO 80307-3000. (wcollins@ucar.edu; eaton@ucar.edu; pjr@ucar.edu)

B. V. Khattatov and J.-F. Lamarque, Atmospheric Chemistry Division, National Center for Atmospheric Research, P.O. Box 3000, Boulder, CO 80307-3000. (boris@ucar.edu, lamar@ucar.edu)

C. S. Zender, Earth System Science, 216 PSRF, University of California, Irvine, CA 92697-3100. (zender@uci.edu)

(Received April 27, 2000; revised July 28, 2000;
accepted August 14, 2000.)